FREQUENCY DOMAIN ANALYSIS OF A LCC TYPE RESONANT CONVERTER

by

TRIPTA THAKUR

DEPARTMENT OF ELECTRICAL ENGINEERING
INDIAN INSTITUTE OF TECHNOLOGY KANPUR
MARCH, 1995

FREQUENCY DOMAIN ANALYSIS OF A LCC TYPE RESONANT CONVERTER

A Thesis Submitted

In Partial Fulfilment of the Requirement

for the Degree of

MASTER OF TECHNOLOGY

by

TRIPTA THAKUR

to the

DEPARTMENT OF ELECTRICAL ENGINEERING
INDIAN INSTITUTE OF TECHNOLOGY KANPUR
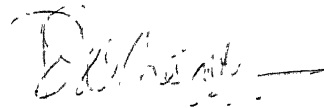
March, 1995

DEDICATED TO
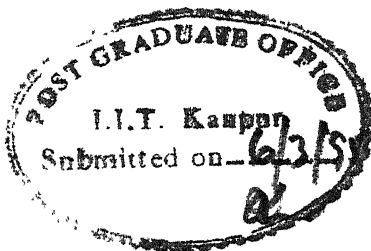
MY

PARENTS

EE-1995-M-THA-FRE

CERTIFICATE

This is to certify that the thesis entitled "FREQUENCY DOMAIN ANALYSIS OF A LCC TYPE RESONANT CONVERTER" by Tripta Thakur has been carried out under our supervision and that this work has not been submitted elsewhere for a degree.

Dr. B. G. Fernandes
Assistant Professor
Dept. of Elect. Engg.
Indian Institute of Technology
Kanpur - 208016

Dr. S.R. Doradla
Professor
Dept. of Elect. Engg.
Indian Institute of Technology
Kanpur - 208016

ACKNOWLEDGEMENT

various stages of this thesis.

I take this opportunity to express my heartfelt gratitude to all members of my family, who have always stood by me. Their constant support, encouragement, love and complete trust in me has enabled me to work towards achieving success. My special thanks goes to my husband Mr. Mukul Kulshrestha, Lecturer, Department of Civil Engineering, REC Bhopal, for his constant moral support.

My sincere thank to Mr. J.P. Gupta who has helped in typing this thesis.

Lastly, I wish to thank all those who have directly or indirectly helped me throughout my work.

<div align="right">TRIPTA THAKUR</div>

CONTENTS

ABSTRACT

In this thesis the steady state analysis of LCC resonant converter is carried out using the frequency domain model. Pulse width modulation is employed to control the output voltage. Based on the analysis, a simple design procedure is given. Detailed SPICE simulation results are presented for the designed converter to evaluate its performance for load variation. The converter presented oprates in lagging power factor mode for a very wide variation in the load. This converter is suitable for high voltage output applications.

CHAPTER 1

INTRODUCTION

1.1 INTRODUCTION

High frequency dc-to-dc resonant converters have been steadily increasing since 1980's, in order to achieve smaller size, lighter weight and faster transient response. Soft switching features of resonant converters make them desirable for high frequency, high power applications.

Resonant converters are classified into two types, series resonant converters (SRC) and parallel resonant converter (PRC) depending on the manner in which energy is extracted from the resonant tank. The SRC uses the resonant inductor current and PRC uses resonant capacitor voltage to transfer energy from tank to the load. Both SRC's and PRC's are thoroughly analysed in the literature [1],[5]. It has been observed that while dealing with higher order topologies the acronym series or parallel donot mean much since energy could be extracted by the load in series with the resonant inductance and still using parallel resonant circuit and vice versa. There is no widely accepted definition of classifying resonant converters into series or parallel connections. Hence, for generalization purposes, only the term resonant converters are normally used in the literature.

The SRC operates optimally when the switching frequency (f_s) is the same as the resonant frequency (f_o) and the performance of SRC is load dependent. The PRC has low efficiency at light load due to higher circulating currents and cannot take short circuit loads. It also exhibits load dependent operation. Also, SRC and PRC need to be operated over wide range of frequencies to get full control of the output voltage. Fig. 1.1 shows the transfer curves of SRC and PRC.

In order to overcome the limitations listed earlier, fixed frequency operation with various control techniques as given below were tried

(i)   Fixed frequency with phase staggering control [5]-[7].

(ii)   Fixed frequency with pulse width strategy [8]-[10].

(iii)   Fixed frequency with integral cycle control (Quantum Control) [11]-[12].

All the above mentioned control techniques use some sort of feedback to gain the control over the resonant converters, over a wide range of load and input voltage variations. With the exception of a few topologies the majority of the existing topologies, whether full bridge, half bridge or single ended quasi resonant are of second order resonant circuit where the storage tank consists of only two energy storage elements. Recently there has been growing interest in the area of high frequency converters, which provide load independent operation. The addition of third resonant element modifies input-output

2

RESONANT CONVERTERS < Transfer Curves >
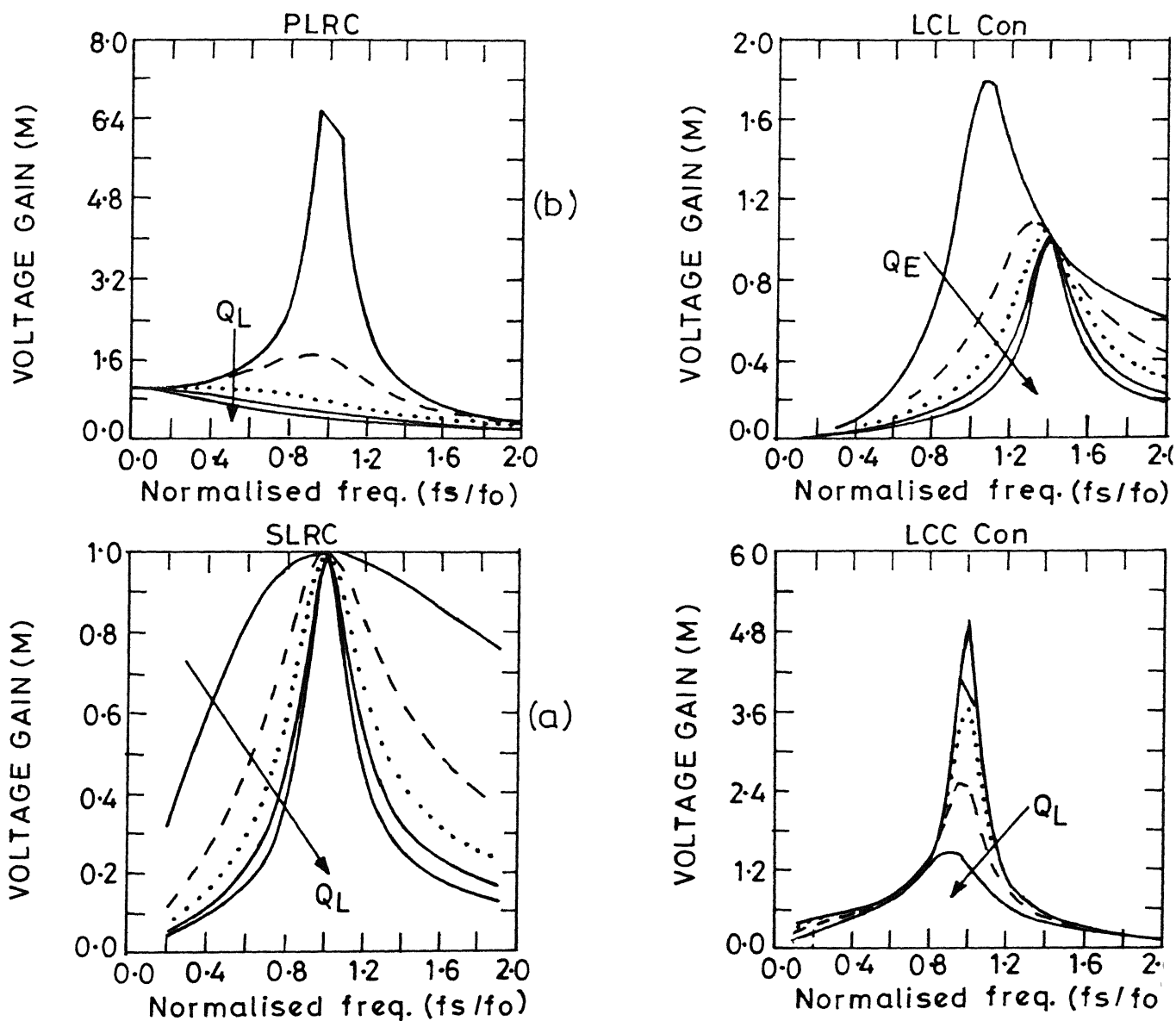
Fig.1·1   Transfer characteristics of resonant converters
(a) SLRC (b) PLRC (c) LCC converter (d) LCL converte

characteristics substantially resulting in load independent operation (Fig. 1.1). An LCC resonant converter is very similar to a parallel resonant converter (PRC), except that a series capacitor is added to the resonant tank. A properly designed LCC resonant converter has less current stress than a PRC, because LCC converter combines the advantage of series resonant converter (SRC) and parallel resonant converter (PRC). Therefore, LCC resonant converters are also called series-parallel resonant converters (SPRC's).

The parasitic L and C associated with the load and the hf transformer forces the standard two element topology to practically operate as three or four elements. As a result, the parasitic reactance can turn into an asset rather than liability. The advantages of three element topologies are :

(i)   Load independent operation.

(ii) The output voltage can be made either higher or lower than the input voltage depending on the configuration and the reactance ratio.

(iii) Diversity in resonant topologies gives the designer the freedom to choose the topology that suits the operation.

The only drawback of higher order converter is that their steady state analysis becomes more difficult.

1.2 SELECTION OF RESONANT TOPOLOGY

The possible three element configurations are discussed in detail in [13]. It was suggested in [13] that the power

converters can be partitioned into three blocks as shown

```
┌──────────┐     ┌──────────┐     ┌──────────┐
│  Source  │     │ Resonant │     │   Load   │
│   V/I    │─────│ Network  │─────│   V/I    │
└──────────┘     └──────────┘     └──────────┘
   Block 1          Block 2          Block 3
```
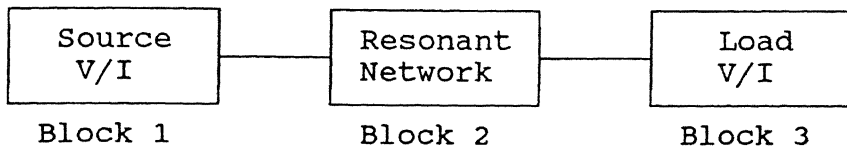
The blocks 1 and 3 are selected from the considerations of input and output requirements. Block 2, which represents the resonant topology is designed to meet specific requirements. Thirty eight 3-element topologies and their compatibility with input and output requirements have been listed [13]. Each topology is identified with four letters. The first letter represent the type of source (V or I), the second letter represents the resonant network (N), the third letter represents the type of load (V or I) and the last letter indicates whether the converter is resonant or not. For example, VNV-R means, the resonant network compatible with voltage type of source and voltage type of load.

For regulating the output voltage in a resonant converter the most common method is the frequency control. If operation is below resonance (leading p.f.), then the switching frequency (f_s) is reduced to very low values at light loads. This results in an increased size for the magnetic components in addition to the problem such as the need for lossy RC snubbers, di/dt limiting inductors etc. By operating resonant converters above resonance (lagging p.f.), the need for lossy snubbers and di/dt inductors is eliminated. However, the switching frequency needed

for light loads is very high. This increases the magnetic core losses and also poses problems in the design of control circuit. Because of these disadvantages of frequency control, PWM control is attempted in power supplies which have varying loads.

In this thesis LCC (also called as series-parallel) resonant dc-to-dc converter is studied, which gives load independent operation. This is desirable, which is built into most power supplies. The LCC resonant dc-to-dc converter provides the best characteristics of the SRC and PRC while eliminating their drawbacks (high ripple current in dc filter capacitor for the SRC and circulating current independent of load for the PRC). Because of the disadvantages of frequency control, fixed frequency PWM control technique is used to get load independent operation. Converter is operated above the resonance frequency (lagging p.f.).

1.3 OBJECTIVE

Basically three methods are available for analysing resonant converter in steady state.

(i)   Approximate analysis using complex a.c. circuit analysis [14],[15].
(ii) State space or differential equation approach [16].
(iii) Fourier series method or frequency domain approach [17], [18].

All these methods of analysis employed a time domain

approach which involved solution of differential equations by numerical integration. Steady state analysis using differential equation requires considerable computational effort. When the steady state analysis is desired, the frequency domain approach is comparatively more efficient.

The following are the advantages of frequency domain analysis over other methods of analysis

(i)   All harmonics are taken into account, analysis is simple and gives good result.

(ii)   In the complex ac circuit analysis, although the method is simple the results are not quite accurate, particularly when the switching frequency is away from the resonant frequency or as the duty ratio decreases.

(iii) SLRC and PLRC need to be operated over wide range of frequency to get full control of the output voltage. In order to overcome the problems of variable frequency operation of resonant converters they are operated at a constant frequency with the voltage controlled by PWM technique.

(iv)   The converter operates in lagging power factor (above resonance) mode for a very wide change in the load currents as well as the supply voltage.

The parallel resonant converter (PRC) and series resonant converter (SRC) were analysed by using a frequency domain model [18],[21]. An attempt is made to analyse a three element

resonant converter using frequency domain approach in this thesis. LCC resonant converter is choosen for the analysis. Various circuit variables are determined by simple expressions. The steady state analysis is thus considerably simplified.

The objective of the thesis are achieved in different chapters as outlined here. Chapter 2 presents the modelling and operation of the converter in different modes. Steady state analysis using frequency domain approach is done in chapter 3. Simulation of the converter with SPICE-3 package is presented in chapter 4. Some guidelines in the selection of component values and their ratings are given in chapter 5, with an illustrative example.

CHAPTER 2

LCC RESONANT DC TO DC CONVERTER

In this chapter, the operating principle, modelling and various possible modes of operation in one cycle of operation are described.

2.1 CIRCUIT DESCRIPTION

The basic circuit diagram of LCC type series resonant converter is shown in Fig. 2.1. S_1-S_4 are switching devices having base or gate turn off capability. D_1-D_4 are anti-parallel diodes across the device. These can be internal diodes of MOSFET's. MOSFET together with antiparallel diodes acts as a bi-directional switch. The positive portion of the current flows through the switch and negative portion of the current flows through diode. L_s, C_s and C_p are the resonant series inductor, capacitor and parallel resonant capacitor respectively. In this circuit, to make use of the leakage inductance of the high frequency transformer, the parallel resonant capacitor is placed on the secondary side of the transformer [20]. R_L represents the resistive load.

The switching frequency is kept constant and power control is obtained by phase shifting the gating signals to vary the pulse width (δ). The converter is designed to operate with maximum pulse width ($\delta = \Pi$) when the load current is maximum and
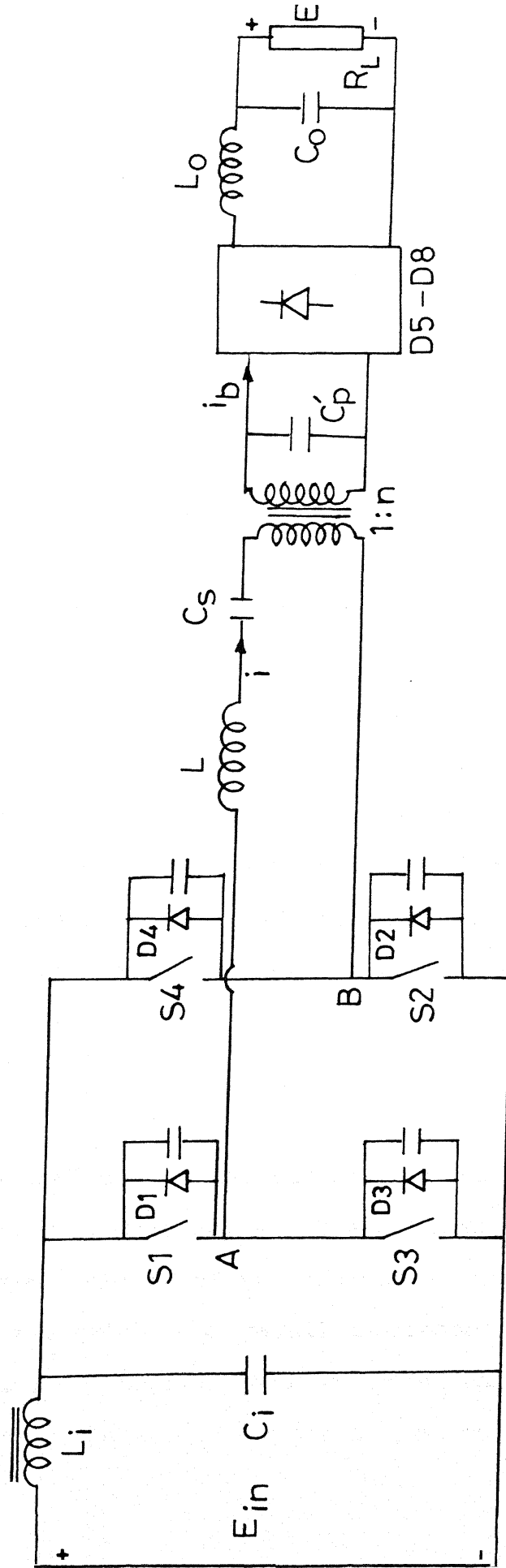
Fig. 2·1 Basic circuit diagram of LCC Resonant DC to DC Converter.

the supply voltage is minimum. The phase shift 'ϕ' between the gating signals is controlled to regulate the load voltage with variations in the load current or in the input supply voltage. As the load current decreases to regulate the output voltage, the pulse width is decreased by phase shifting the gating signals G_2 and G_4 respectively with respect to G_1 and G_3, as shown in Fig. 2.2.

Depending on the switching frequency the equivalent reactance across the terminal AB may be capacitive or inductive. The fact that the circuit is operating above resonance (lagging p.f.) can be deduced from the fact that the current delivered to the resonant circuit (that is the current in series inductor (L_s)) is lagging the voltage applied to the resonance circuit (V_{AB}). It is given in [3] that the operation of resonant converters above resonance is the proper choice for most power supply applications operating at high frequencies. Therefore, the analysis to follow are all done for operation above resonance.

2.2 OPERATING MODES

To simplify the analysis of the circuit and to have better understanding of circuit operation, all the devices are assumed to be ideal. The turns ratio of hf transformer is assumed to be unity. Each MOSFET alongwith the parallel connected internal diode is represented by a pair of bidirectional switches. The voltage across terminals AB, 'V_{AB}' depends on the switching
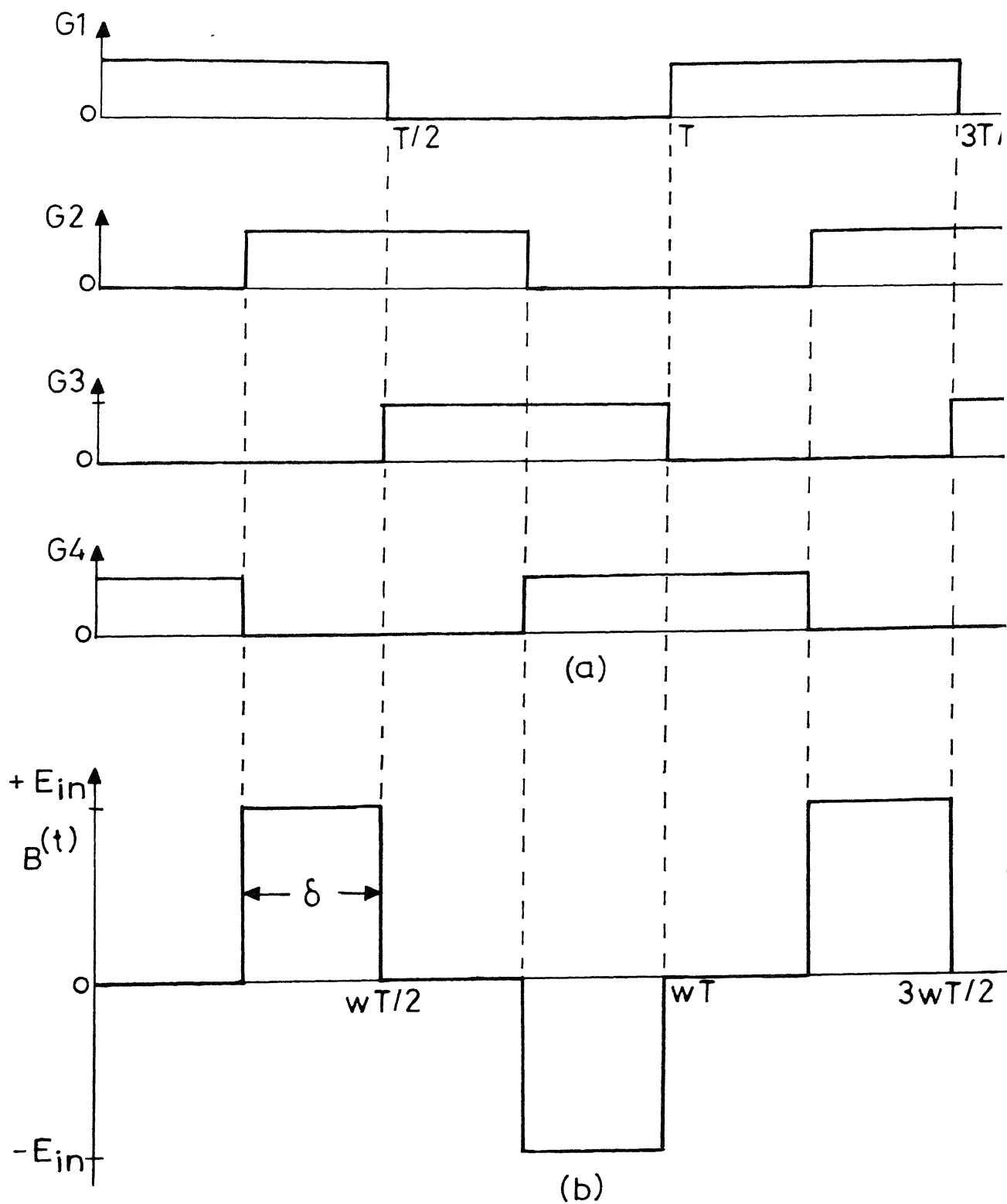
G1

G2

G3

G4

(a)

$+E_{in}$

$B^{(t)}$

δ

$wT/2$

O

wT

$3wT/2$

$-E_{in}$

(b)

Fig. 2·2   (a) Gating signals to switches

(b) $v_{AB}(t)$

status of the switches. When the gating signal G_1 is present then,

$$V_{AB}(t) = +E_{in} \qquad \text{if } G_2 \text{ is also present}$$
$$= 0 \qquad \text{otherwise.}$$

Similarly, $V_{AB}(t) = -E_{in}$ or 0 depending upon the switching status of G_3 and G_4. Thus the effect of the switching devices can be represented as a equivalent voltage source $V_{AB}(t)$, as shown in Fig. 2.3. "P" assumes the values +1, 0 and -1 depending on the switching status as explained above. Fig. 2.3 also represents the equivalent circuit of Fig. 2.1.

Under steady state conditions, the resonant converter may operate in one of the possible 5 different modes of circuit operation which are called Mode 1 to Mode 5, depending upon the status of $V_{AB}(t)$ and $V_{CP}(t)$. When pulse width is maximum (Duty ratio, D=1), the resonant converter can operate in two different modes namely Mode 1 and Mode 2. Under reduced pulse width (D<1), the converter can operate in three more different modes (Mode 3 to Mode 5). Based on the operating waveforms and the equivalent circuit model (Fig. 2.3) the operation of the converter in different identified modes is explained below.

MODE 1

This mode occurs with full pulse width ($\delta=\Pi$) or (D=1). Inductor current i_L or series current, i(t) lags behind the voltage applied to the tank, thus converter operates in lagging
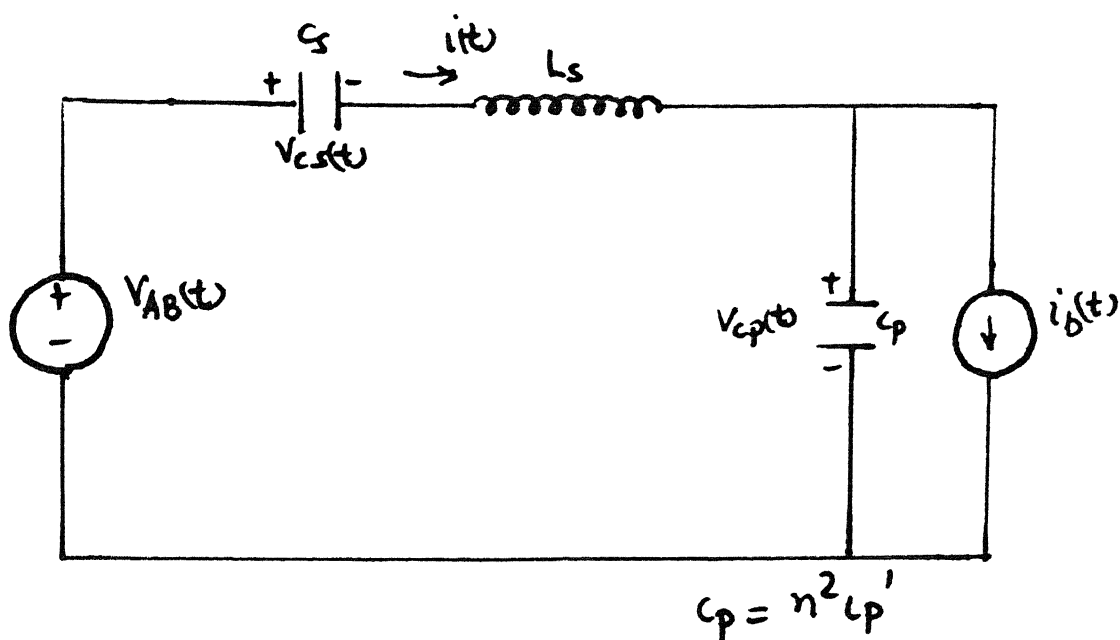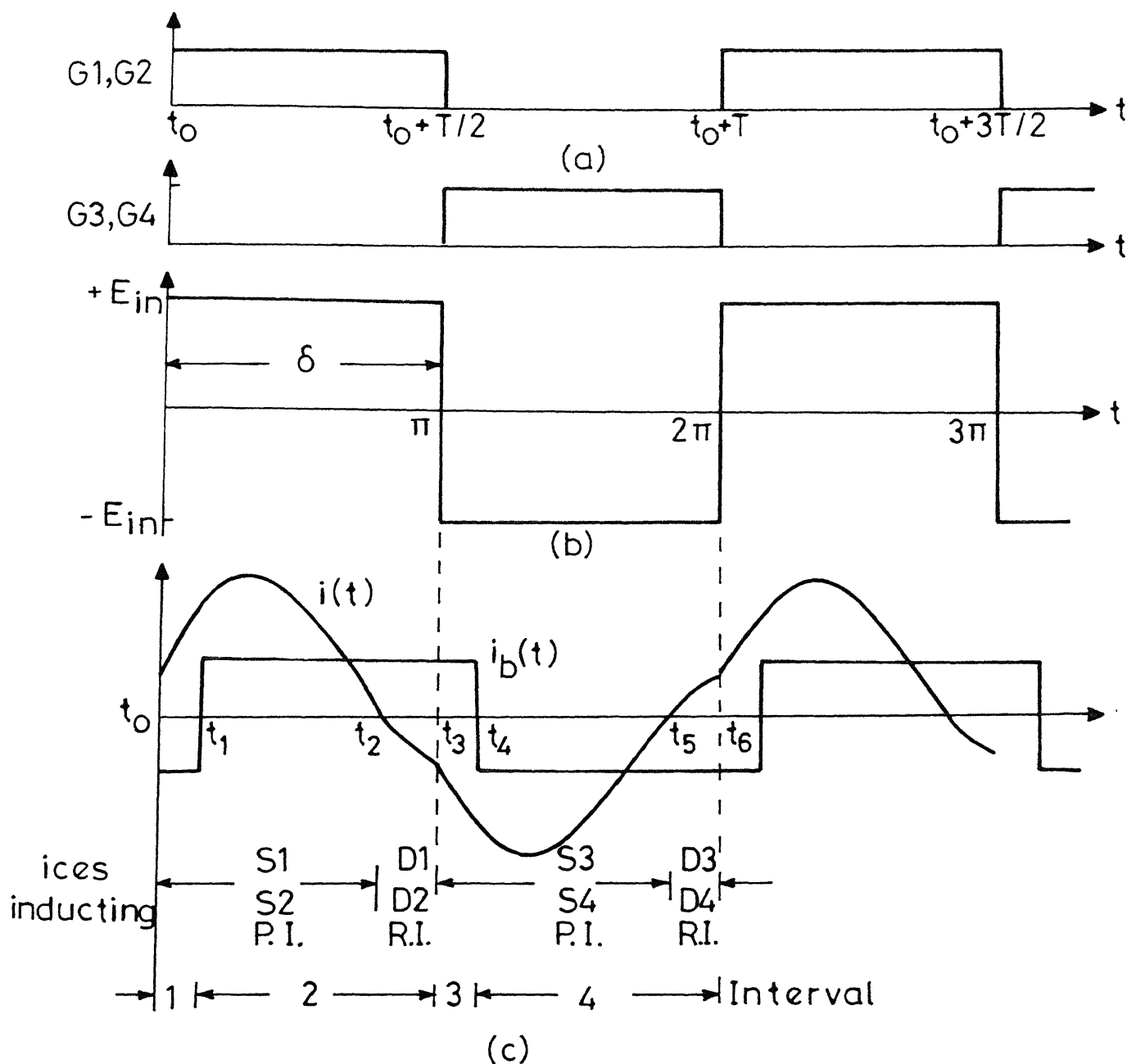
Fig. 2.3 : Equivalent circuit of Fig. 2.1

P. I.- Power Interval
R.I.- Regenerative Interval

Fig. 2·4 MODE 1 typical operating waveforms
   (a) Gating signals G1 to G4
   (b) $v_{AB}(t)$
   (c) $i(t)$ and $i_b(t)$

15

p.f. mode. There are four intervals of operation in each cycle. Fig. 2.4 shows the typical waveform for this mode of operation. At steady state, both resonant capacitor voltage (not shown in the figure) and resonant inductor current will have initial values as switches S_1 and S_2 are turned on at $t=t_o$. The tank voltage becomes $+E_{in}$ immediately. In internal, 1 $i_b(t)$ is negative. The transition from interval '1' to '2' takes place at $t=t_1$. When the capacitor voltage $V_{CP}(t)$ (not shown in the figure) changes its sign. The resonant current will reach zero at $t=t_2$, and S_1 and S_2 are natually commutated. Therefore zero current turn off is realised. As the resonant current reverses at t_2, with the tank connected to $+E_{in}$, D_1 and D_2 turn on allowing a part of the tank energy to return to the source during the time interval t_2-t_3. The converter operates in the interval '2' till $t=t_3$. At this instant S_3 and S_4 are turned on and therefore V_{AB} changes from $+E_{in}$ to $-E_{in}$. The converter now operates in interval '3'. At $t=t_4$, V_{CP} changes its sign gradually from positive to negative and the interval '4' begins. This interval ends at $t=t_5$. When i(t) becomes zero and begins to reverse, forcing diodes D_3 and D_4 to conduct. The interval t_2-t_3 and t_5-t_6 are called Regenerative Interval (R.I.) and the interval t_o-t_2 and t_3-t_5 are called Power Interval (P.I.). Thus in this mode there are two power and two regenerative intervals.

As the switches turn on at finite current and at a finite voltage, this results in turn on switching power loss. Thus mode

1 operation requires lossy snubbers and di/dt limiting inductors.

MODE 2

This mode occurs with full pulse width ($\delta=\Pi$) or (D=1). Fig. 2.5 shows typical waveform for this mode of operation. It is evident from Fig. 2.5 that diode D_1 and D_2 are conducting initially at $t=t_0$. When the current through diodes reaches zero (at $t=t_1$), switches S_1 and S_2 are turned on and the current is transferred from the antiparallel diodes. The converter operates in interval '1' till $t=t_2$. There is no voltage across switches at turn on (since D_1 and D_2 are conducting), which eliminates turn on losses and facilitates operation of the switches with lossless snubbers. At $t=t_2$, the transition from interval '1' to interval '2' takes place. At $t=t_3$ when the switches S_1 and S_2 are turned off, the current is transferred to D_3 and D_4. Turn off losses are present in such type of operation, because during turn off, current and voltage are simultaneously present at the switch. The sequence of events repeat in the next half cycle. The interval t_0-t_1 and t_3-t_4 are called regenerative interval while t_1-t_3 and t_4-t_6 are called power intervals.

MODE 3

Fig. 2.6 shows the operationg waveforms of this mode. At $t=t_0$, $i(t)$ is negative, therefore D_1 conducts. During the interval t_0-t_1, the current freewheels through S_4, resonant tank, D_1 and back to S_4. This interval is called freewheeling
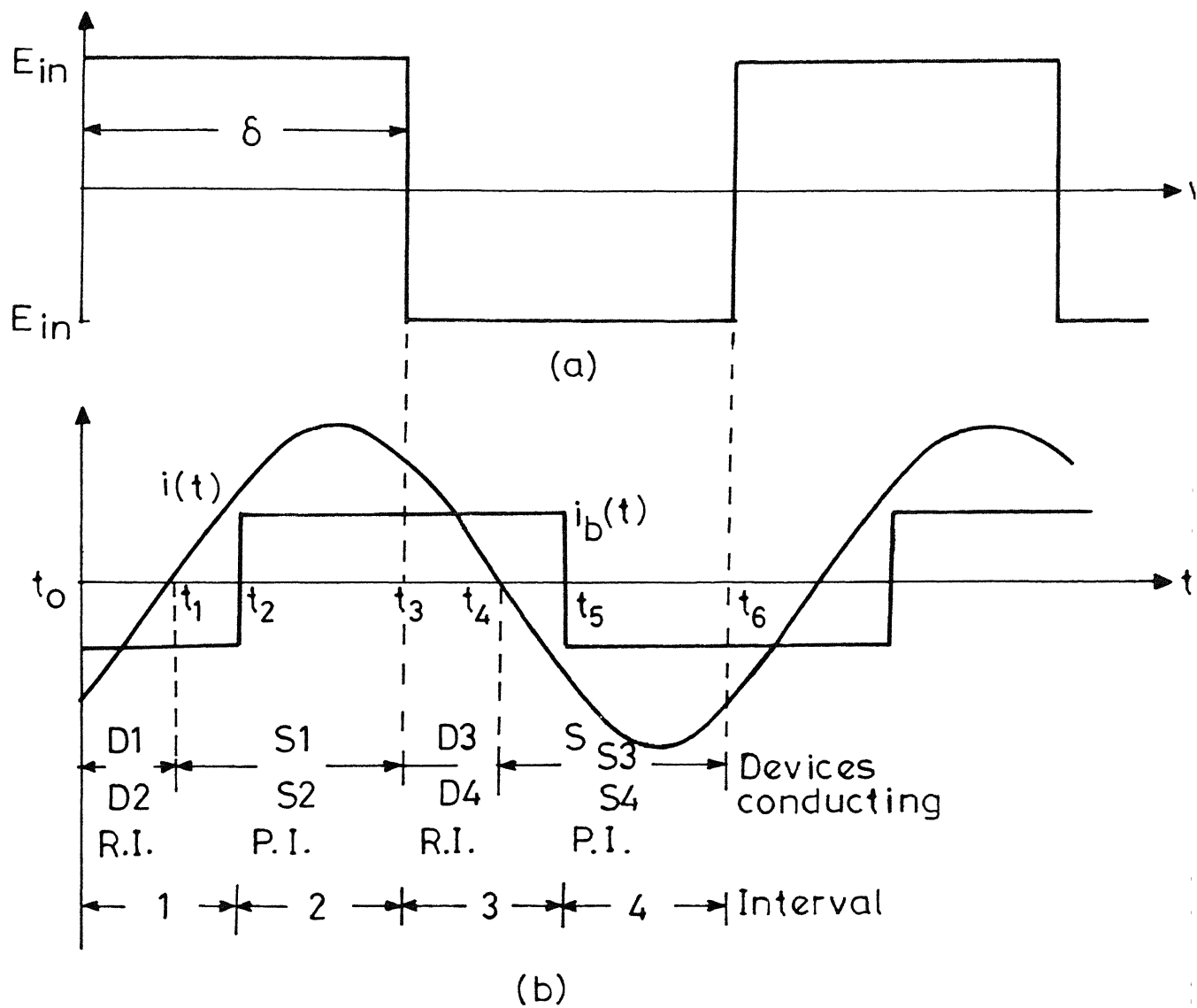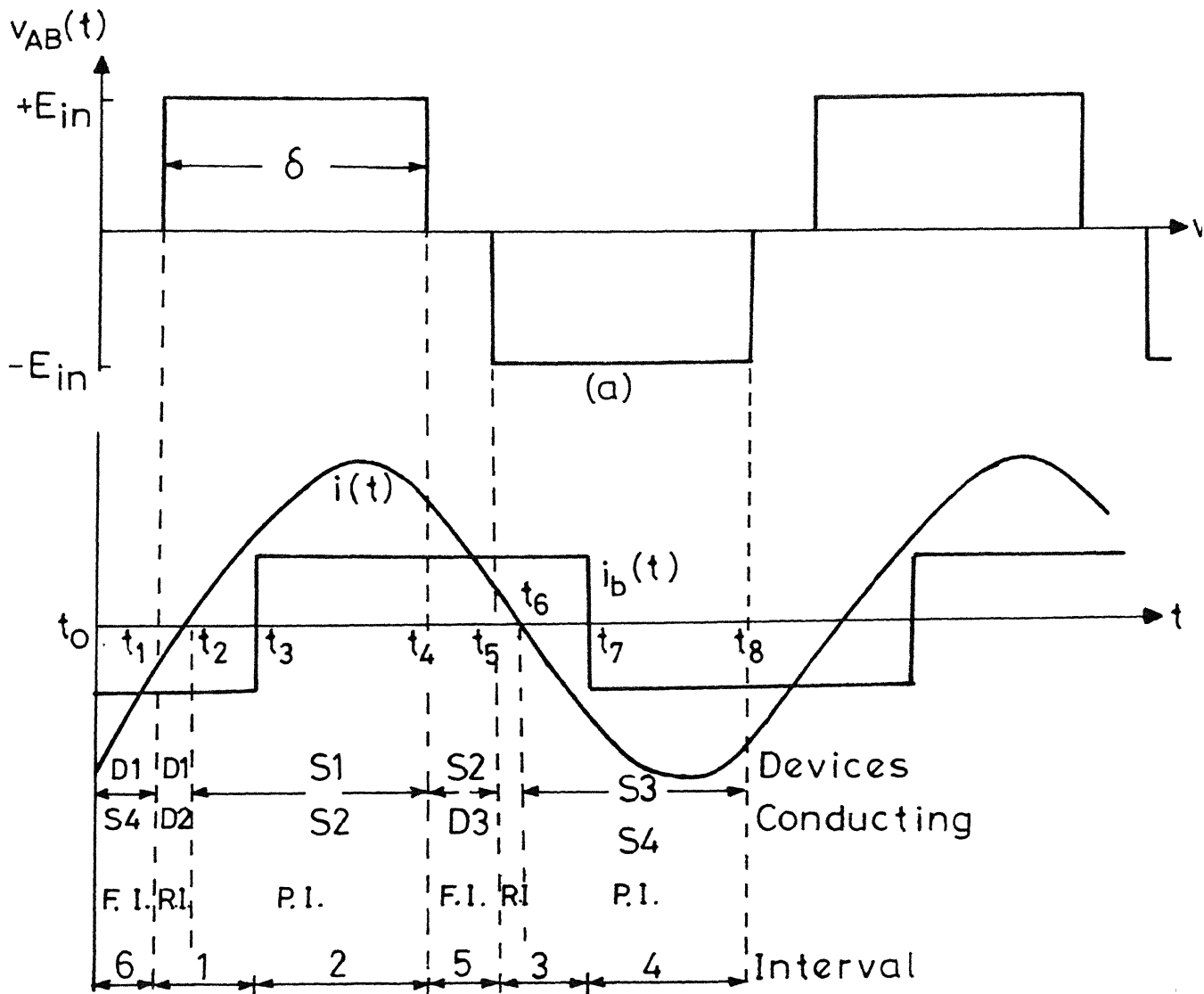
Fig. 2·5 MODE 2 typical operating waveforms

(a) $V_{AB}(t)$

(b) $i(t)$ and $i_b(t)$

18

F. I. - Freewheeling interval

Fig. 2·6   MODE 3 typical operating waveforms
         (a) $v_{AB}(t)$
         (b) $i(t)$ and $i_b(t)$

interval (F.I.). At $t=t_1$, the transition from interval '6' to interval '1' takes place. In this interval '1' initially D_1 and D_2 conducts, transferring the energy in the inductor back to source. As a result, $i(t)$ reduces to zero and S_1 and S_2 starts conducting. This makes the beginning of power interval. At $t=t_3$, $i_b(t)$ changes from negative to positive and the converter operation changes from interval '1' to interval '2'. The power interval ends at $t=t_4$. The sequence of events repeat in the next half cycle and the converter transits from interval '1' to interval '2'. The power interval ends at $t=t_4$. The sequence of events repeat in the next half cycle and the converter transits from interval '2' – '5' – '3' – '4' – '6'. It may be noted that in this mode also all switches turn on at zero voltage, facilitating use of lossless snubbers.

MODE 4

Fig. 2.7 shows the operating waveform for this mode of operation. As in the mode of '3', the various operating intervals in this mode can also be explained. It can be observed that the switches S_1 and S_3 turn on with zero voltage across them (at $t=t_1$ and $t=t_5$ respectively), whereas the switches S_2 and S_4 requires lossy snubbers and di/dt limiting inductors. Also, the diodes D_2 and D_4 must have fast recovery characteristics. The switches S_1 and S_3 are forced to turn off at $t=t_4$ and $t=t_8$ respectively.

MODE 5

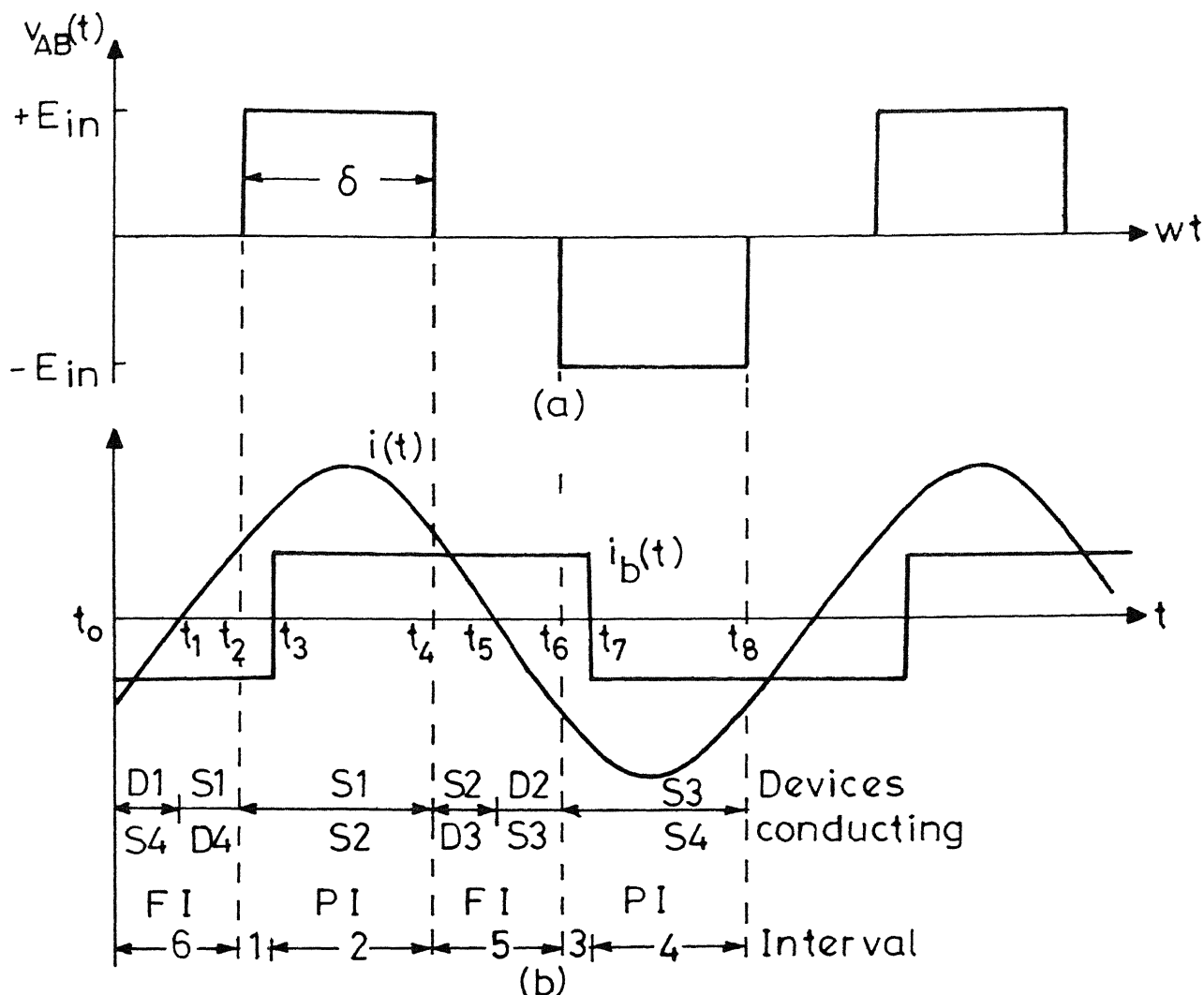Fig. 2·7   MODE 4 typical operating waveforms
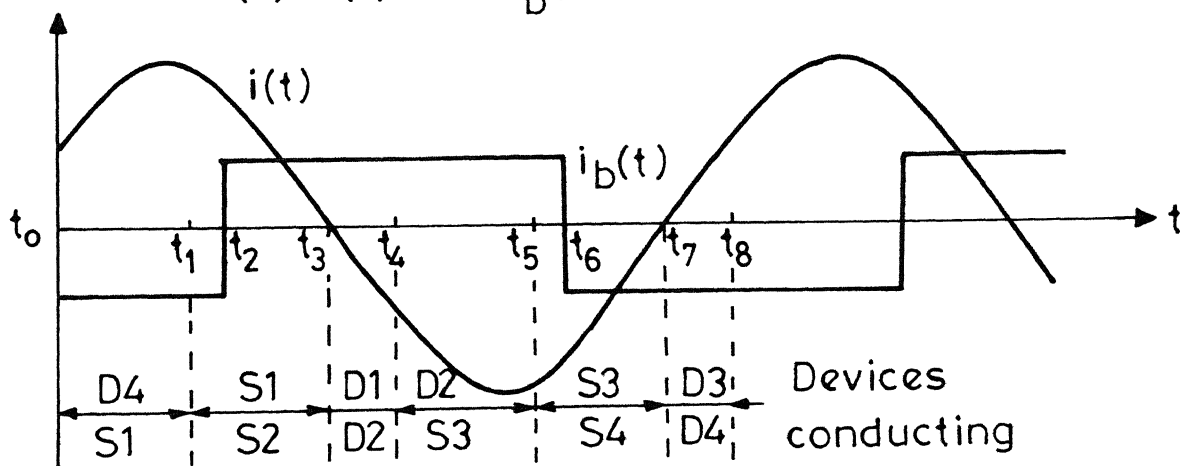(a) $v_{AB}(t)$
(b) $i(t)$ and $i_b(t)$

Fig. 2·8   MODE 5 typical operating waveforms
$i(t)$ and $i_b(t)$

21

The operating waveforms for this mode are shown in Fig. 2.8. It can be seen that all the switches turn on at finite voltage and finite current. Therefore, the switches have to be provided with RC snubbers and di/dt limiting inductors.

In this section, all the possible modes in which converter can operate have been discussed. This discussion is aimed to understand how the switches and/or diodes operate in a cycle of operation. It is also evident from the above discussion that the above resonance operation in preferable compared to below resonance operation. By choosing proper switching frequency with respect to series (or parallel) resonance frequency, operation in any of these modes is possible.

CHAPTER 3

ANALYSIS

3.1 ANALYSIS PROCEDURE

Three analysis methods are available for analysing resonant converter in steady state

(i)   Approximate analysis using complex a.c. circuit analysis - In this method fundamental components of the waveforms are used for voltage and current. This method is not an accurate method and when switching frequency is away from resonance frequency accuracy will further reduced.

(ii)   Steady state or differential equation approach - This method is accurate and gives good results, with lower order converter, but analysis becomes complicated and very combersome with higher order converters.

(iii) Fourier series method - In this method, all the harmonics are taken into account and classical a.c. circuit analysis techniques are used to analyze the converter. Therefore this method is simple and gives good results.

The analysis presented in this section uses the frequency domain approach and is based on the following assumptions -

(i)   Ideal input d.c. voltage.

(ii)   The switching and diodes used in the converter are ideal.

(iii) The resonating element L, C_s and C_p are lossless.

(iv)   Effect of snubbers is neglected.

(v)   The high frequency transformer is ideal and has unity

turns ratio.

(vi)   Load voltage is assumed to be constant so that constant voltage source model can be used.

BASE VALUES

All the equations used are normalized using the following base values

$$V_B = E_{in}(min)$$

$$Z_B = \left(\frac{L_s}{C_s} \right)^{1/2}$$

$$I_B = \frac{V_B}{Z_B}$$

Equivalent circuit for LCC resonant converter is shown in Fig. 3.1(a), where $C_p = n^2 C_p$.
C_p is the equivalent capacitor referred to the primary and 'n' is the number of turns.

NOTATIONS USED

All the normalized quantities are denoted by extra subscript 'o' and the subscript 'n' denotes n^{th} harmonics component. The normalized reactance for nth harmonic is

$$\text{Total series reactance } X_{sno} = X_{Lsno} - X_{Csno}$$

$$X_{sno} = \left(nF - \frac{1}{nF} \right) \text{ p.u.} \qquad (3.1)$$

where F is frequency ratio.

Total parallel reactance $X_{pno} = \dfrac{1}{nF} \left(\dfrac{C_s}{C_p} \right)$ p.u.

or

$$X_{pno} = \frac{m}{nF} \text{ p.u.} \qquad (3.2)$$

where m is the ratio of C_s and C_p.

$$X_{eqno} = X_{sno} \, X_{pno} \, / \, X_{sno} + X_{pno} \qquad (3.3)$$

Let the converter gain be denoted by M, then

$$M = \frac{\text{Output voltage referred to the primary side}}{\text{Base voltage}}$$

$$M = \frac{V'_o}{V_B}$$

where

$$V'_o = \frac{V_o}{n}$$

Normalized load current $= \dfrac{nI_d}{I_B}$ $\qquad (3.4)$

EXPRESSIONS FOR VOLTAGE AND CURRENTS

Voltage V_{AB} applied to the resonant tank is of the form shown in Fig. 3.1(b). The duty ratio, D is defined as the ratio of the time duration for which S_1 and S_2 or S_3 and S_4 are switched on simultaneously (t_{ON}) to the half of the switching period (T/2),

$$D = \frac{t_{ON}}{T/2} \qquad (3.5)$$

so δ and D are related by,

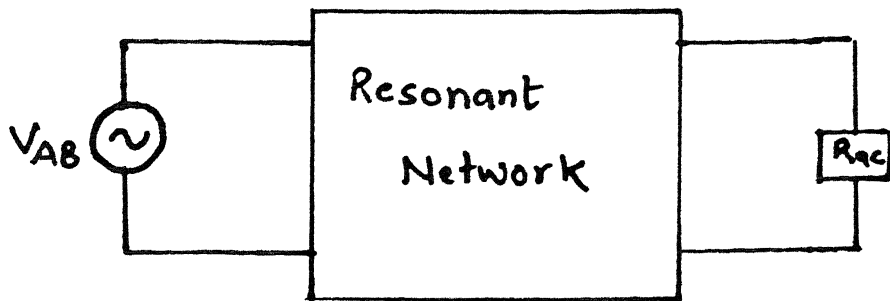$$\delta = \Pi.D \text{ rad.} \qquad (3.6)$$

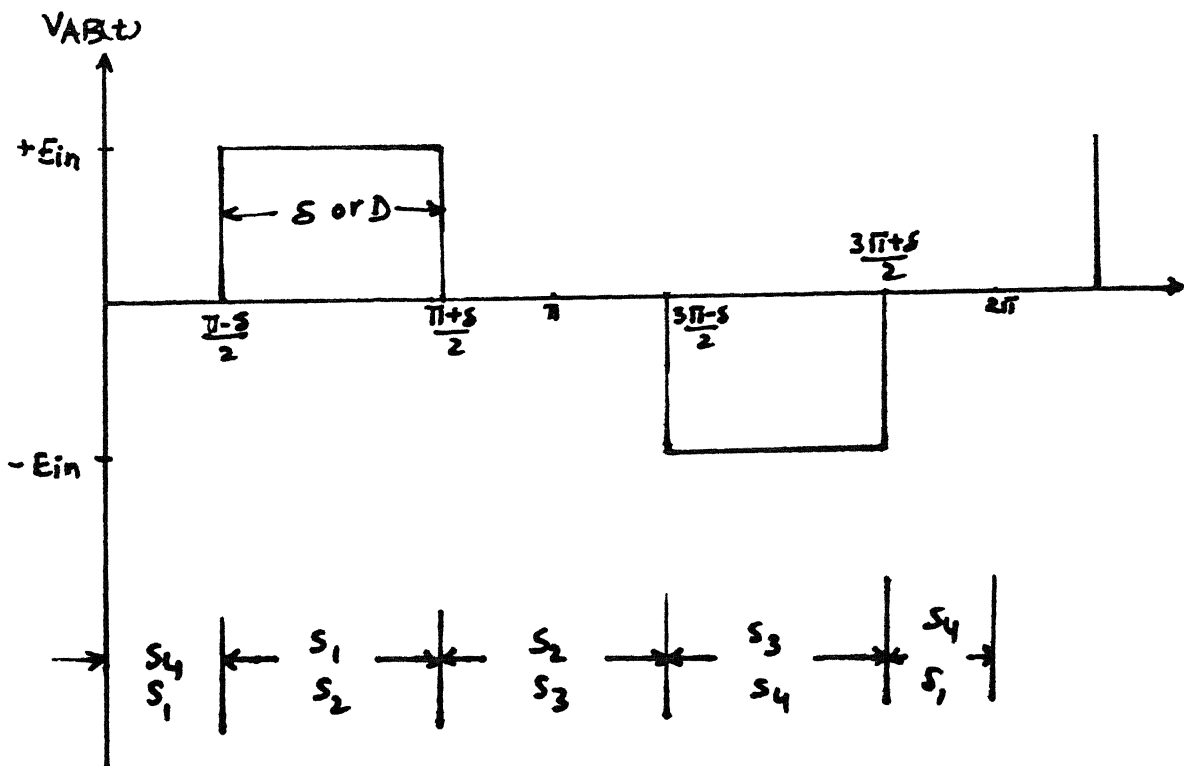Fig. 3.1(a) : Equivalent circuit for LCC resonant converter

Fig. 3.1(b) : Voltage applied to the resonant tank (V_{AB})

The square wave voltage across AB can be calculated by Fourier Series Analysis

$$a_n = 0$$

$$F(\theta) = \sum_{n=1}^{\infty} b_n \sin(n\theta)\ d\theta$$

$$b_n = \frac{2}{\Pi} \int_{\Pi-\delta/2}^{\Pi+\delta/2} E_{in} \sin\theta\ d\theta$$

$$b_n = \frac{2E_{in}}{\Pi} \left[-\frac{\cos n(\frac{\Pi+\delta}{2})}{n} + \frac{\cos n(\frac{\Pi-\delta}{2})}{n} \right]$$

$$b_n = \frac{2E_{in}}{\Pi} \left[-\frac{\cos \frac{n\Pi}{2} \cdot \cos \frac{n\delta}{2}}{n} + \frac{\sin \frac{n\Pi}{2} \cdot \sin \frac{n\delta}{2}}{n} \right.$$

$$\left. + \frac{\cos \frac{n\Pi}{2} \cdot \cos \frac{n\delta}{2}}{n} + \frac{\sin \frac{n\Pi}{2} \cdot \sin \frac{n\delta}{2}}{n} \right]$$

$$b_n = \frac{4E_{in}}{\Pi} \frac{\sin(\frac{n\Pi}{2})\ \sin(\frac{n\delta}{2})}{n} \qquad (3.7)$$

$$V_{AB} = \sum b_n \sin n\omega_{st}\ dt$$

From eqn. (3.7)

$$V_{AB} = \frac{4}{\Pi} \sum \left[\sin \frac{(n\omega_{st})}{n}\right]\left[\sin(\frac{n\Pi}{2})\right]\left[\sin(\frac{n\delta}{2})\right]\ \text{p.u.} \quad (3.8)$$

The summation $\sum$ shown for the fourier series represents sum of odd harmonics, i.e. n = 1,3,5,...

Let V'_o be the voltage at the input of the rectifier bridge referred to the primary side

$$V'_{oo} = \frac{4M}{\Pi} \sum \frac{\sin(n\omega_{st} - n\theta)}{n} \quad p.u. \tag{3.9}$$

where 'θ' is the phase shift of voltage V'_o from t=0.

For calculating KVA rating of tank and stress on various element, it is necessary to calculate rms current, voltage which is calculated as follows by calculating instantaneous values of current and voltage through resonating element.

Fig. 3.2(a) shows equivalent circuit for nth harmonics at terminal AB. By using superposition theorem Fig. 3.5(a) can be split into Fig. 3.2(b) and 3.2(c). The instantaneous current through the resonating inductor L_s is given by

From Fig. 3 2(b) $\quad I_{Lsn1} = \dfrac{V_{ABn}}{jX_{sn}}$ \hfill (3.10)

and $\quad I_{cpn1} = 0$ \hfill (3.11)

From Fig. 3.2(c) $\quad I_{Lsn2} = \dfrac{V'_{on}}{jX_{sn}}$ \hfill (3.12)

$I_{Lsn} = I_{Lsn1} + I_{Lsn2}$ (by using superposition theorem).

From Fig. 3.10 and 3.12

$$I_{Lsn} = \frac{V_{ABn}}{jX_{sn}} + \frac{V'_{on}}{jX_{sn}} \tag{3.12}$$

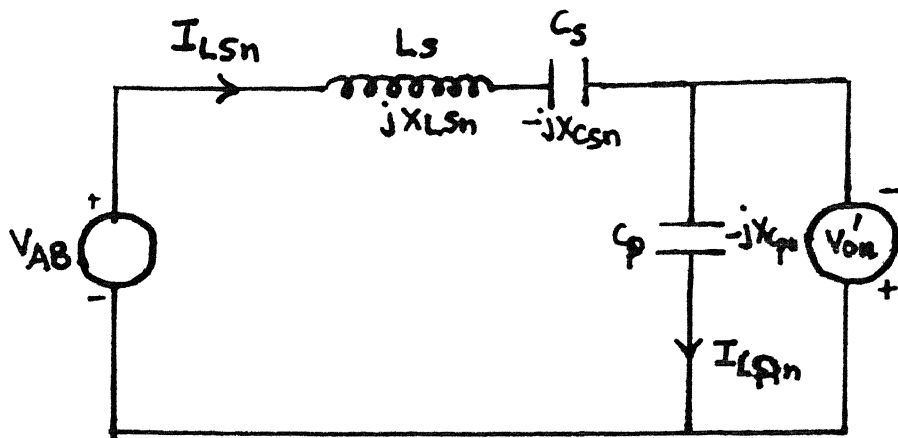By putting value of V_{ABn} and V'_{on} from (3.8) and (3.9) respecti-

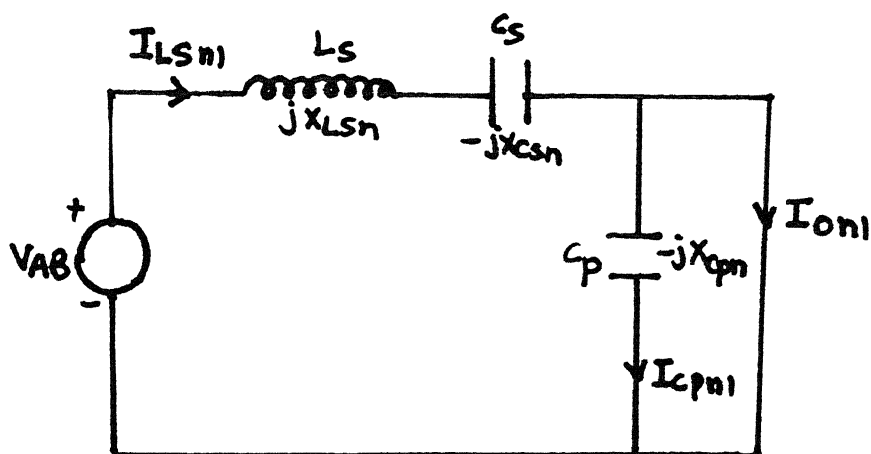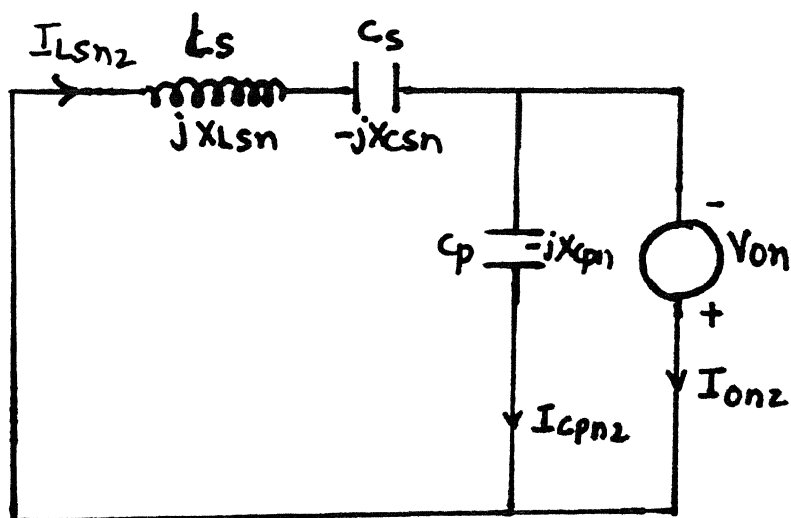Fig. 3.2(a) : Equivalent circuit for n^{th} harmonics at terminal AB

Fig 3.2 (b)

Fig. 3.2(b) and c : Equivalent circuit for applying superposition theorem

vely in (3.12)

$$I_{Lsno} = \frac{-4}{\Pi} \sum \left[\frac{\cos(n\omega_{st})}{nX_{sno}}\right]\left[\sin(\frac{n\Pi}{2})\right]\left[\sin(\frac{n\delta}{2})\right]$$

$$+ \frac{4M}{\Pi} \sum \left[\frac{\cos(n\omega_{st} - n\theta)}{nX_{sno}}\right] \tag{3.13}$$

Simplifying (3.13)

$$I_{Lsno} = \frac{-4}{\Pi} \sum \left[\frac{\cos(n\omega_{st})}{nX_{sno}}\right]\left[\sin(\frac{n\Pi}{2})\right]\left[\sin(\frac{n\delta}{2})\right]$$

$$+ \frac{4M}{\Pi nX_{sno}} \sum \left[\cos(n\omega_{st})\right]\left[\cos(n\theta)\right] + \left[\sin(n\omega_{st})\right]\left[\sin(n\theta)\right]$$

Taking $\cos(n\omega_{st})$ term and calling it I_{Lspn10}

$$I_{Lspn10} = \frac{4}{\Pi}\left[\frac{-\sin(\frac{n\Pi}{2})\sin(\frac{n\delta}{2}) + M\cos(n\theta)}{nX_{sno}}\right] \tag{3.14}$$

And taking $\sin(n\omega_{st})$ term and calling I_{Lspn20}

$$I_{Lspn20} = \frac{4M}{\Pi}\frac{\sin(n\theta)}{nX_{sno}} \tag{3.15}$$

$$I_{Lspno} = \left[I_{Lspn10}^2 + I_{Lspn20}^2\right]^{1/2} \tag{3.16}$$

$$Y_n = \tan^{-1}\left[\frac{I_{Lspn20}}{I_{Lspn10}}\right] \quad \text{radians} \tag{3.17}$$

30

Thus the instantaneous current through resonating element can be written as

$$iL_{so} = \sum I_{Lspno} \sin\left(n\omega_{st} + Y_n\right) \quad \text{p.u.} \tag{3.18}$$

The instantaneous values of voltage across C_s, current through C_p and voltage across L_s are given by

$$V_{csno} = \sum V_{cspno} \cos\left(n\omega_{st} + Y_n\right) \quad \text{p.u.} \tag{3.19}$$

$$iC_{po} = \sum I_{cpno} \cos\left(n\omega_{st} - n\theta\right) \quad \text{p.u.} \tag{3.20}$$

$$V_{Lso} = \sum V_{Lspnco} \sin(n\omega_{st}) + V_{Lspn20} \cos(n\omega_{st}) \quad \text{p.u.} \tag{3.21}$$

where

$$V_{cspno} = - I_{Lspno} X_{csno} \quad \text{p.u.} \tag{3.22}$$

$$I_{cpno} = - \frac{4M}{\Pi} / nX_{cpno} \quad \text{p.u.} \tag{3.23}$$

$$V_{Lspn10} = \left[\frac{4}{n\Pi}\right] \left\{\left[\sin\left(\frac{n\Pi}{2}\right)\right]\left[\sin\left(\frac{n\delta}{2}\right)\right] - M\cos(n\theta)\right\}$$
$$- V_{cspno} \sin(Y_n) \tag{3.24}$$

$$V_{Lspn20} = \left[\frac{4}{n\Pi}\right]\left[M\sin(n\theta)\right] + V_{cspno}\cos(Y_n) \tag{3.25}$$

These equations can be used to calculate voltage and current stresses on different components. They are also used to calculate the KVA rating of the tank.

In order to evaluate these equations, the value of 'θ' must

be known. Since the rectifier input voltage changes polarity at $\omega_{st} = \theta$, the diode conducting in the output bridge rectifier changes at 'θ'. The normalised output current is equated to zero at $\omega_{st} = \theta$, to find the angle 'θ'. By using superposition principle for the output current Fig. 3.2(b) and Fig. 3.2(c)

$$I_{on} = I_{on1} + I_{on2}$$

$$I_{on} = \frac{-4}{\Pi} \sum \left[\frac{\cos(n\theta)}{nX_{sno}} \right] \left[\sin(\frac{n\Pi}{2}) \right] \left[\sin(\frac{n\delta}{2}) \right] + \frac{4M}{\Pi} \sum \frac{1}{nX_{eqno}} = 0$$

$$(3.26)$$

The equation (3.26) can be solved numerically to find 'θ' (Newton Raphson technique is used). The initial guess value for 'θ' is obtained from the fundamental component and it is given by

$$\cos(\theta_1) = M \left[1 + \frac{X_{s10}}{X_{p10}} \right] / \sin\left(\frac{\delta}{2}\right) \qquad (3.27)$$

The programme for solving eqn. (3.26) by Newton Raphson technique is given in the Appendix A.

Using the superposition principle for the output current and finding its average value (from Fig.3.2(b) and Fig. 3.2(c)), the normalised load current (J) is obtained and is given by

$$J = \sum \left[\frac{8}{(n\Pi)^2} \right] \left[\frac{\sin(n\theta)}{X_{sno}} \right] \left[\sin(\frac{n\Pi}{2}) \right] \left[\sin(\frac{n\delta}{2}) \right] \qquad (3.28)$$

3.2 DESIGN CURVES

It is important to choose proper values for the resonant

components. Appropriate selection of capacitor ratio (C_s/C_p) and normalised load current (J) results in minimum KVA rating of tank circuit per KW of output power and minimum peak inverter output current at full load. A proper choice of frequency ratio (ratio of switching frequency to series resonance frequency, F) also results in reduced peak currents at light loads while maintianing lagging pf mode of operation. Resonating component values are obtained for the worst case, minimum supply voltage and maximum load current with $\delta=\Pi$.

In (3.28) putting $\delta=\Pi$

$$J = \sum \left[\frac{8}{(n\Pi)^2} \right] \left[\frac{\sin(n\theta)}{X_{sno}} \right] \text{ p.u.} \qquad (3.29)$$

By putting value of X_{sno} from (3.1) in (3.29)

$$J = \frac{8}{\Pi^2} \sum \frac{1}{n^2} \frac{\sin(n\theta)}{\frac{n^2F^2-1}{nF}} \text{ p.u.} \qquad (3.30)$$

$$J = \frac{8}{\Pi^2} \sum_{n=1,3,5,..} \frac{F\sin(n\theta)}{n(n^2F^2-1)} \text{ p.u.}$$

$$J = \frac{8F}{\Pi^2} \left[\frac{\sin\theta}{F^2-1} + \frac{\sin 3\theta}{3(9F^2-1)} + \frac{\sin 5\theta}{5(25F^2-1)} + \ldots \right]$$

General expression for this series can be written as

$$J = \frac{8F}{\Pi^2} \sum_{P=1}^{\infty} \frac{\sin(2P-1)\theta}{(2P-1)\left[\left\{(2P-1)F\right\}^2 - 1\right]} \qquad (3.30)$$

A programme is made to (Appendix B) to solve (3.30). Fig. 3.3 shows normalised load current (J) vs converter gain (M) which is
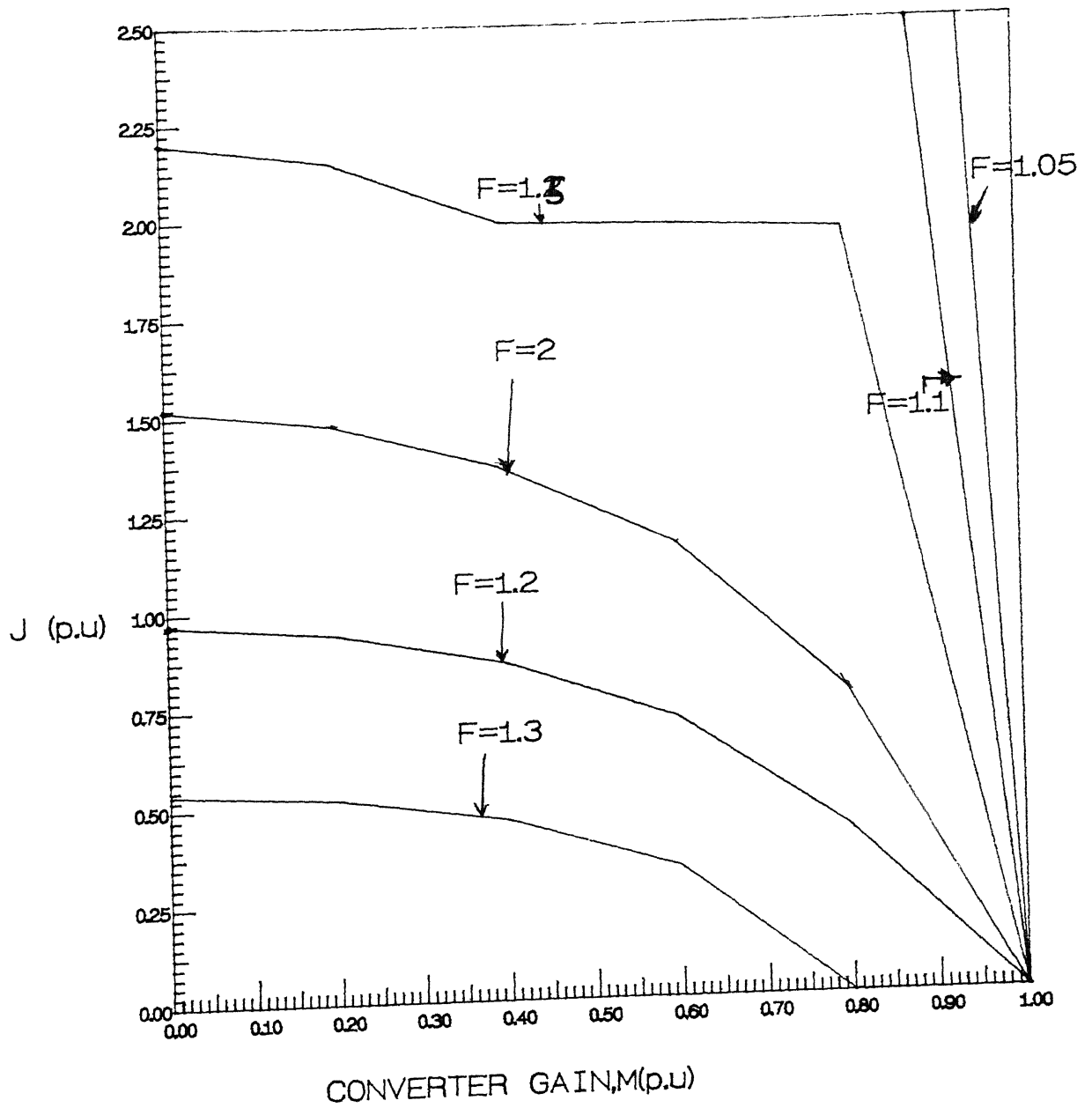
Fig. 3.3 : Normalised Current (J) vs Converter Gain (M)

34

plotted by solving (3.30).

From (3.14), (3.15), (3.16) the peak load current can be calculated

$$I_{Lsro} = \sum \left(I_{Lspno}^2 \right)^{1/2} / \sqrt{2}$$

$$I_{Lspno} = \left(I_{Lspn10}^2 + I_{Lspn20}^2 \right)^{1/2}$$

$$I_{Lsro} = \sum \left(I_{Lspn10}^2 + I_{Lspn20}^2 \right)^{1/2} / \sqrt{2}$$

From (3.15) and (3.16)

$$I_{Lsro} = \left\{ \frac{\sum \left(\frac{4M}{\Pi}\right)^2 \sin^2(n\theta)}{n^2 X_{sno}^2} + \left(\frac{4}{\Pi n X_{sno}}\right)^2 \left\{ 1 + M^2 \cos^2(n\theta) \right.\right.$$

$$\left.\left. - 2M \cos(n\theta) \right\} \right\}^{1/2} / \sqrt{2}$$

$$I_{Lsro} = \frac{4}{\Pi n X_{sno}} \left[\sum M^2 \sin^2(n\theta) + 1 + M^2 \cos^2(n\theta) - 2M \cos(n\theta) \right]^{1/2} / \sqrt{2}$$

$$I_{Lsro} = \frac{4}{\Pi n X_{sno}} \left[\sum 1 + M^2 - 2M \cos(n\theta) \right]^{1/2} / \sqrt{2}$$

$$I_{Lsro} = \frac{4}{2\Pi} \sum \frac{1}{n X_{sno}} \left[1 + M^2 - 2M \cos(n\theta) \right]$$

General expression for this can be written as

$$I_{Lsro} = 0.90F \sum_{P=1}^{\infty} \frac{1 + M^2 - 2M \cos(2P-1)\theta}{\left[(2P-1)^2 F^2 - 1 \right]} \qquad (3.31)$$

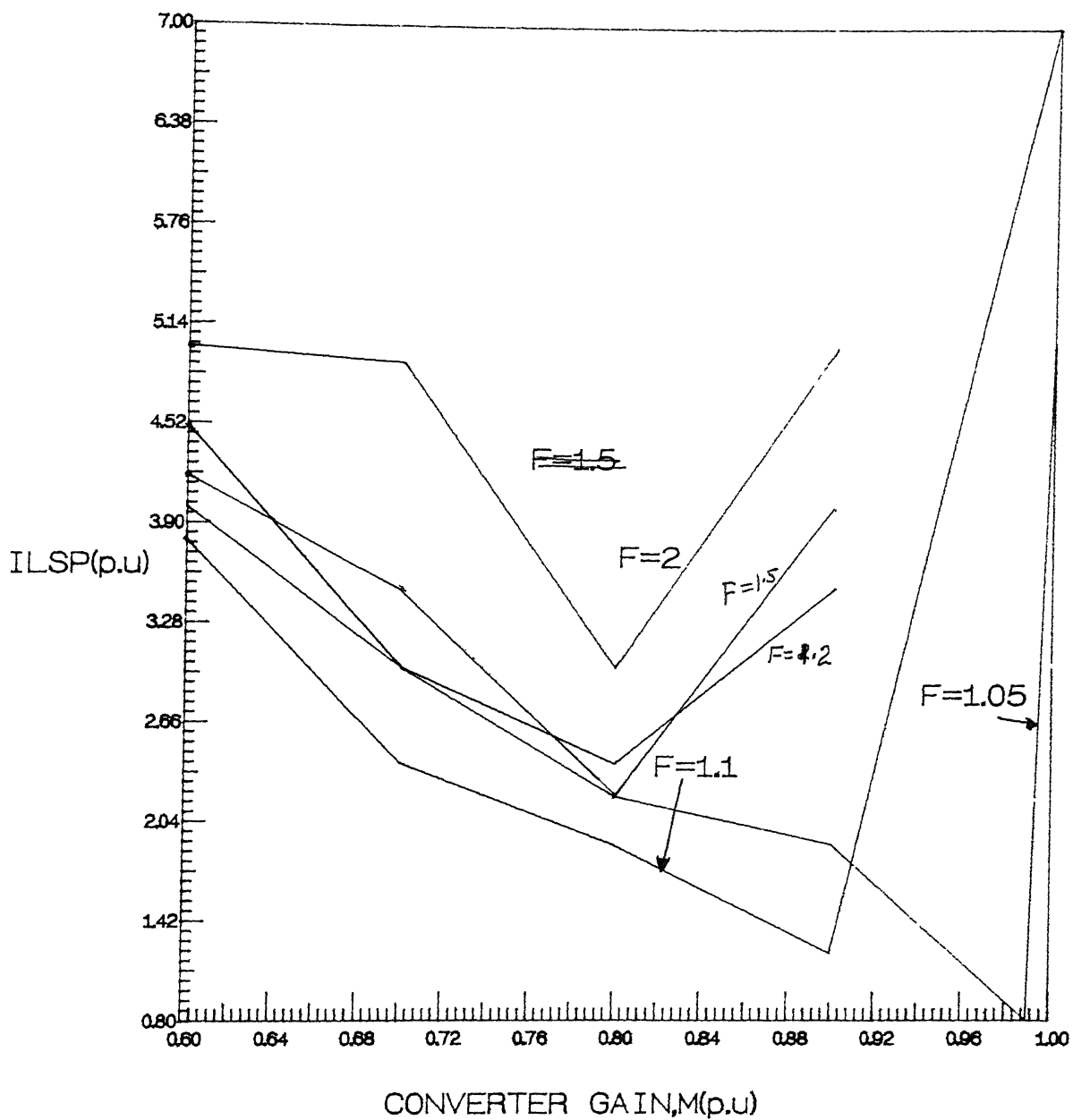A programme is made for solving (3.31) (Appendix B). Fig. 3.4

Fig. 3.4 : Peak inverter load current (I_{Lspn}) vs Converter Gain (M)

:/k : prit

36

shows graph between peak inverter load current (I_{Lspn} vs converter gain (M) which is obtained by solving (3.31). This graph clearly indicates that I_{Lsp} is maximum at light load and it decreases as load increases.

Fig. 3.5 shows the total KVA rating of the tank per KW of output power vs converter gain for $\delta = \Pi$.
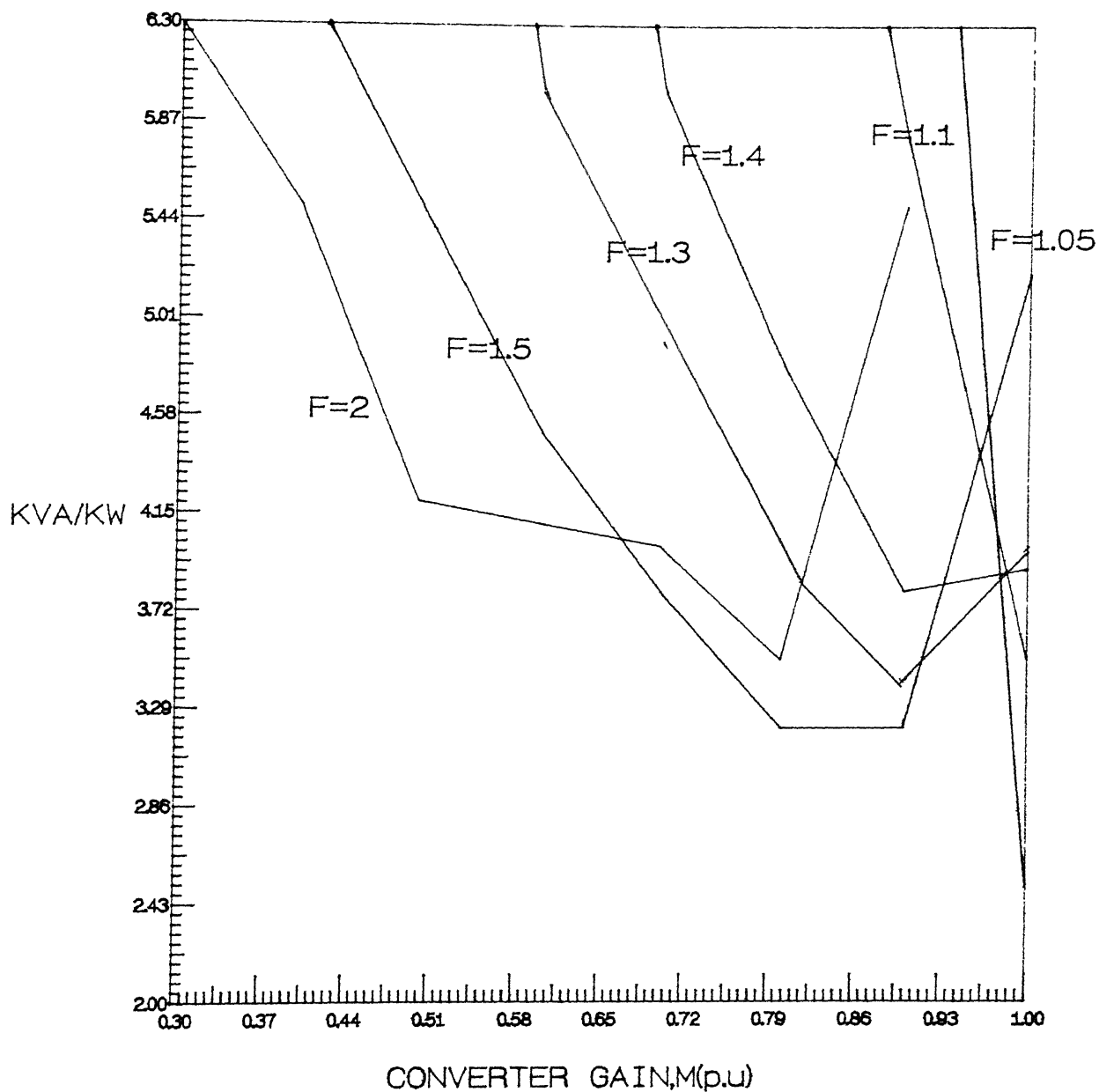
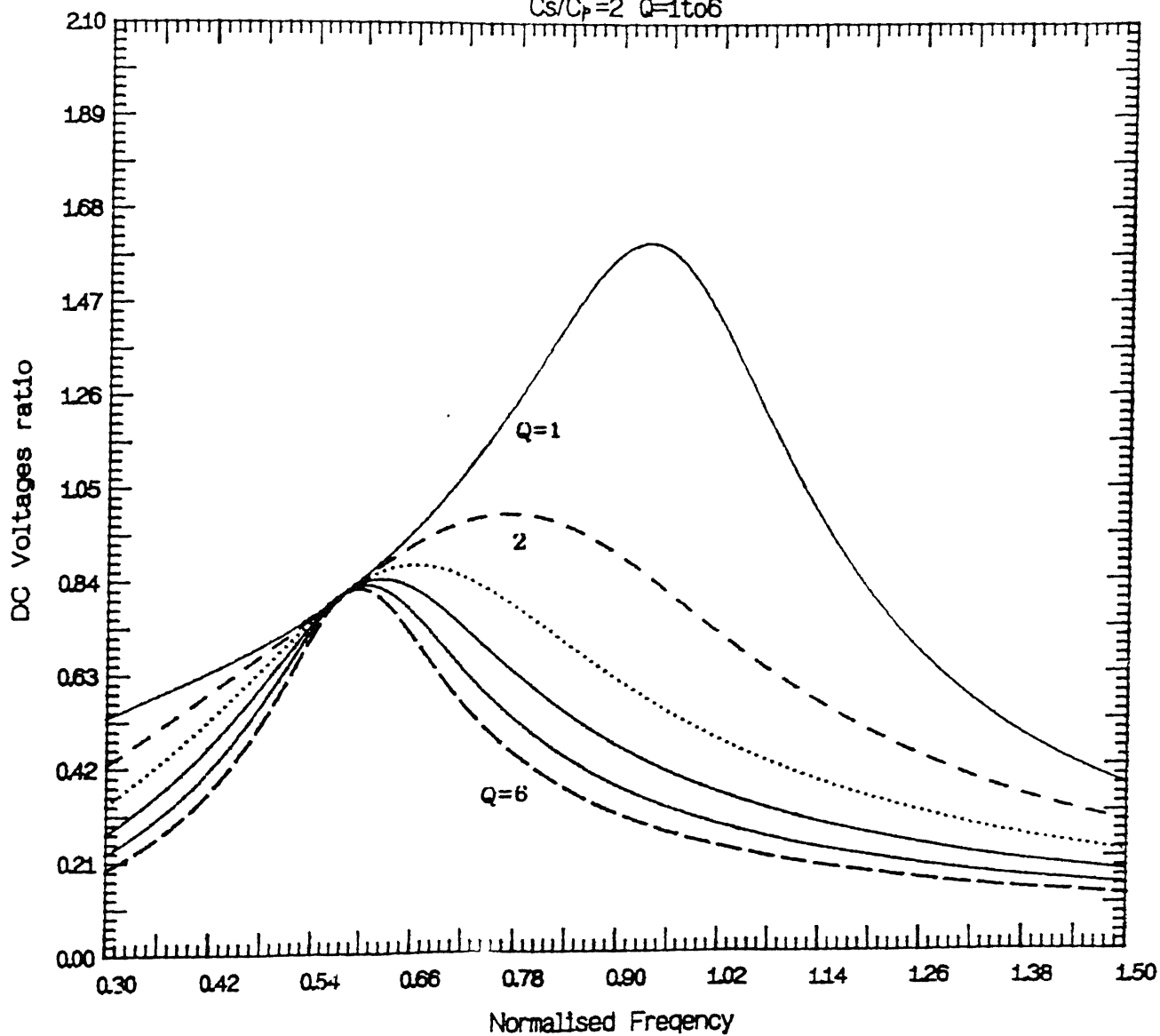Fig. 3.5 : Total KVA rating of the tank per kW of output
power (KVA/kW) vs converter gain (M)

t/k : p

Fig.3.6 Normalised output voltage versus Normalised switching frequency curves for m=2.
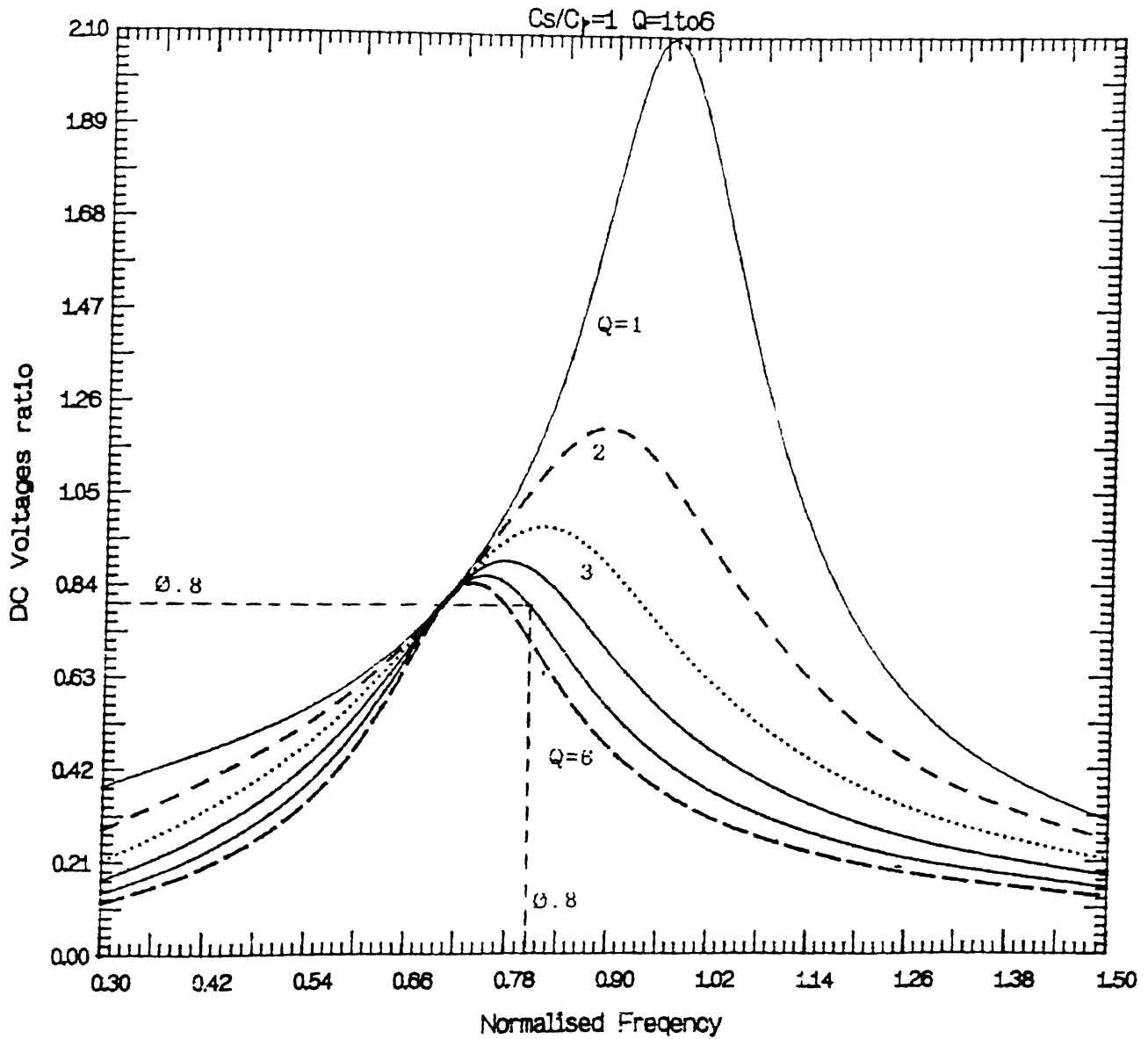
Fig.3.5. Normalised output voltage versus Normalised switching frequency curves for m=1

CHAPTER 4

SPICE SIMULATION

4.1 SPICE SIMULATION

The total LCC converter is simulated using SPICE3 Software Package, which stands for simulation programme with Integrated Circuit Emphasis, software package. SPICE is a general purpose circuit simulation programme for nonlinear dc, nonlinear transient, and linear ac analyses. In the present study, the simulation is aimed to determine the various voltage and current waveforms in the steady state.

Fig. 4.1 gives the circuit diagram used for simulation. current monitoring is done by inserting zero voltage source in series with the branch. Resistance of low values are included in series with all inductors and resistance of high values are connnected in parallel with capacitors to make the simulation network more realistic and also to avoid possible reactance loops. If there is only reactance loop, then the spice simulation is aborted due to non-convergence. Each element in the circuit is specified by an element line that contains the element name, the circuit nodes to which the element is connected and the values of the parameter that determine the electrical characteristics of element.

Fast recovery diodes are simulated by changing the

transient time (tt) parameter of standard diode model. To simulate the power MOSFET, level 1 is used. The transconductance (K_p) and mobility (V_o) of the standard model is changed to get the required MOSFET characteristics close to the manufacture's specifications. Fig. 4.2 gives simulated output characteristics of the MOSFET.

The programme used for transient analysis of the converter is shown in Appendix C. The analysis is carried out over a long period of time of 820 μs and the data is taken during the last cycle of 20 μs. Thus, stable initial conditions are established before taking the data.

The transient analysis is carried out for different duty ratio. Fig. 4.3 to 4.6 gives the simulated waveform of all state variables, input switching waveforms, output switching waveforms and output dc voltage. For each duty ratio, three sets simulation taken for full load, half load 1/3 and 1/4 of load. It is seen from these waveforms that there is very little variation in the output voltage when the load is varied from 20Ω to 80Ω. Whatever the small change overserved in the output voltage may be due to resistance drop across R_o, in series with the load. This resistance is required to be used to avoid the problem of nonconvergence while running the spice software.
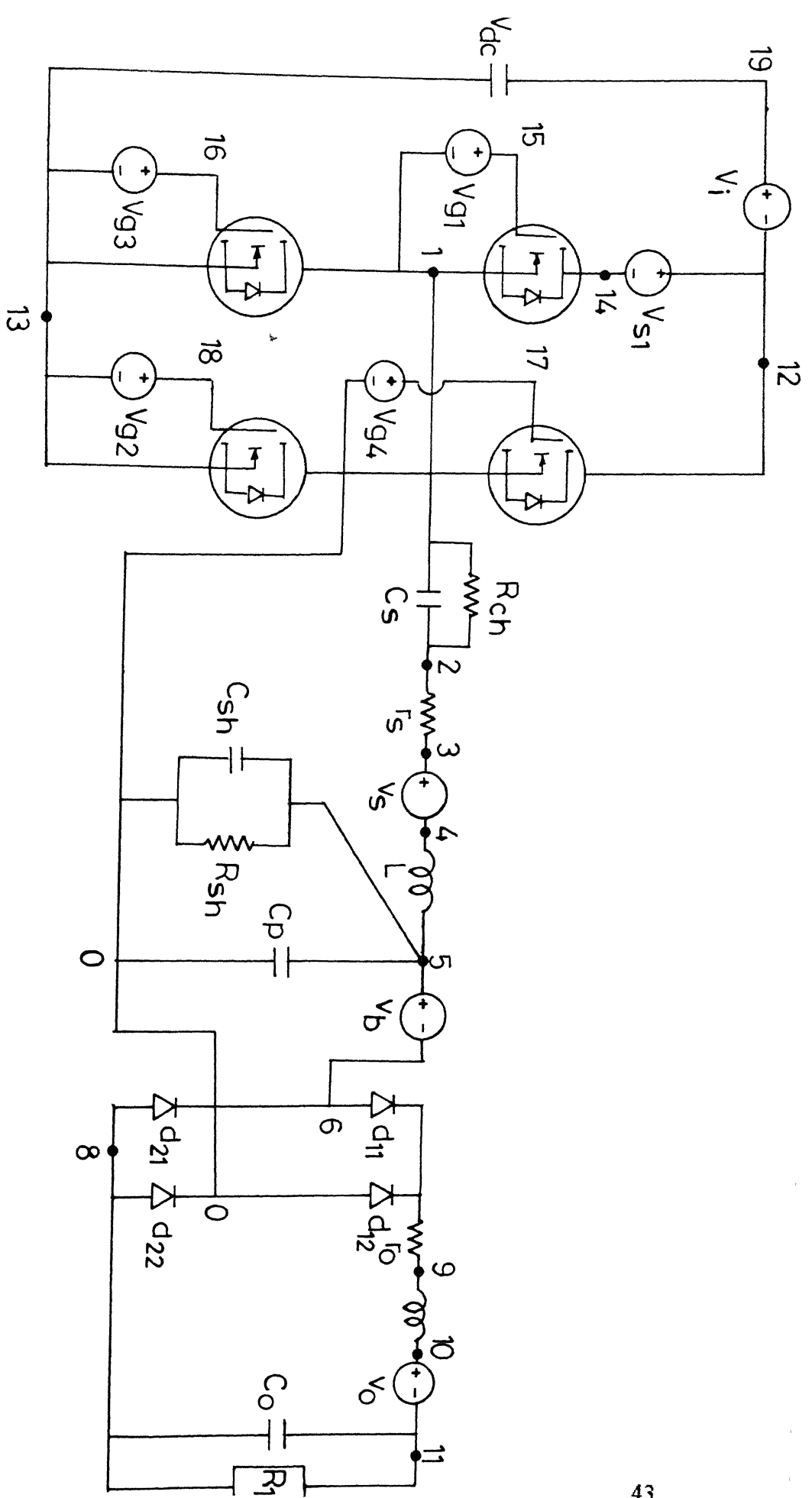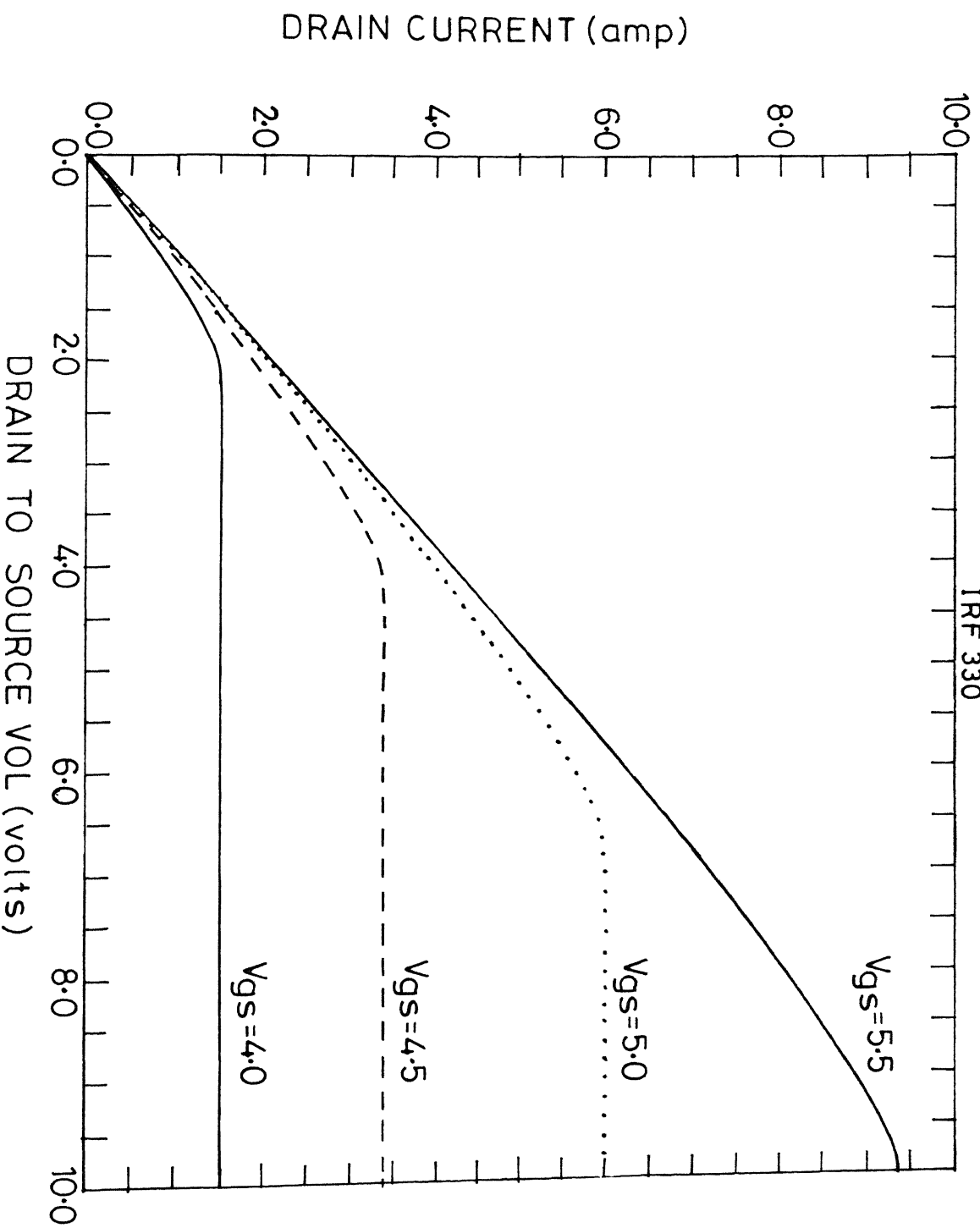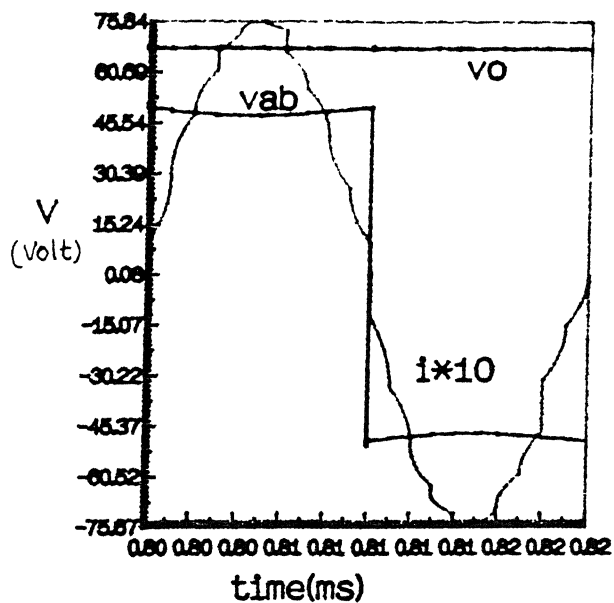
Fig. 4·1 Spice simulation circuit

43

Fig.4·2 Simulated output characteristics of the MOSFET

MOSFET< Output Characteristics >
IRF 330

DRAIN CURRENT (amp)

DRAIN TO SOURCE VOL (volts)

Vgs=4·0

Vgs=4·5

Vgs=5·0

Vgs=5·5

44

D=1 cs=cp=0.16uf ls=76uh
RL=20ohm

D=0.54 cs=cp=0.16uf
ls=76uh RL=40ohm

V
(Volt)

vab

vo

i*10

time(ms)

V
(Volt)

vls

vcs

vcp

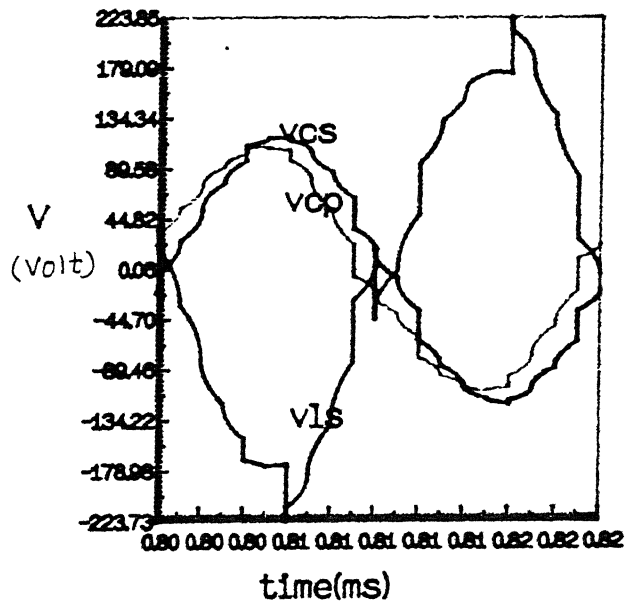time(ms)

vo

vab

i*10

V
(Volt)

time(ms)

vcs

vcp

vls

V
(Volt)

time(ms)
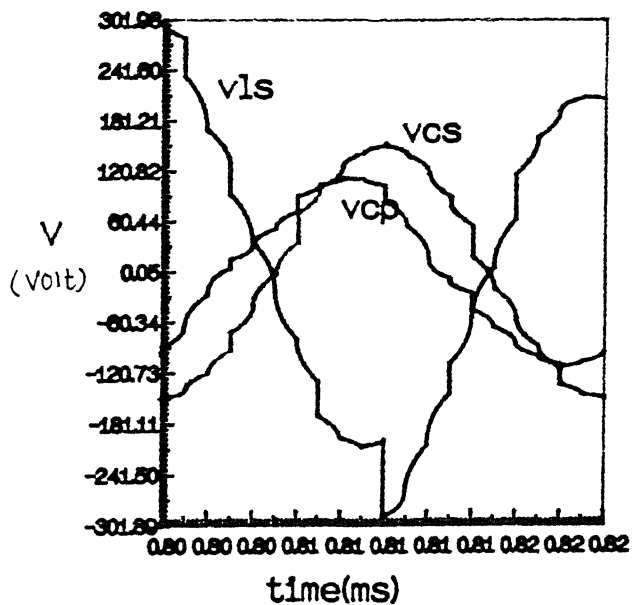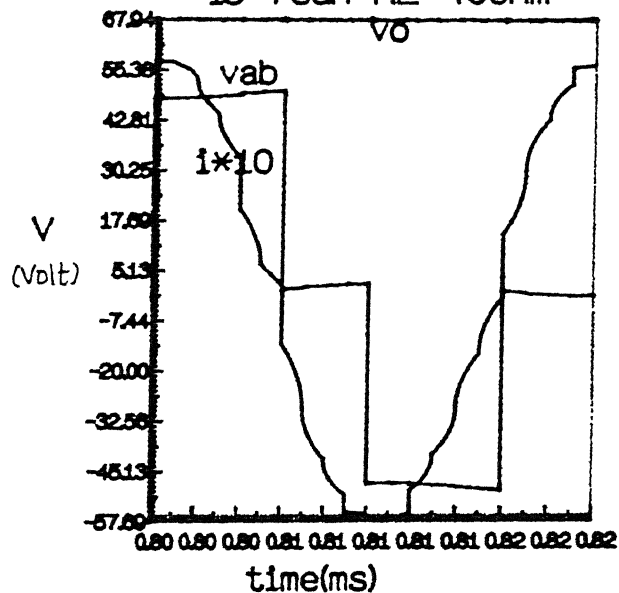
Fig. 4.3 : Simulated waveforms for D=1.0 and D=0.54 E_{in} = 50 V

k : p

45
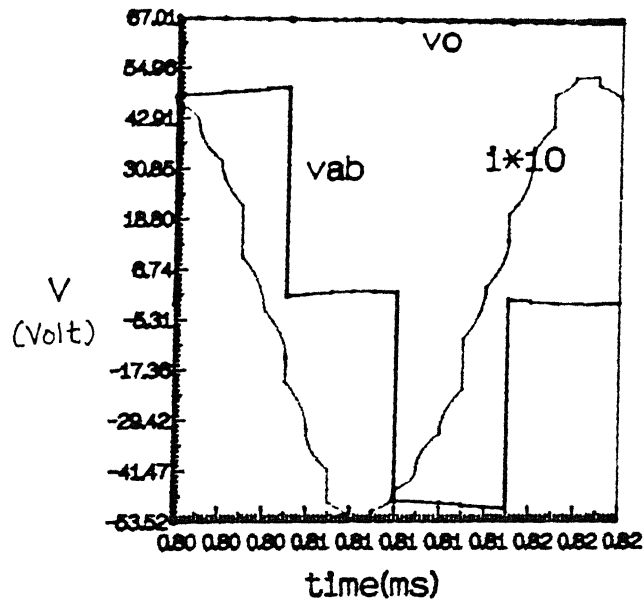
Fig. 4.4 : Simulated waveforms for D=0.5 and D=0.49 E_{in} = 50 V

t/k : pritnvi # 03/04/96 16:01:06 #

46
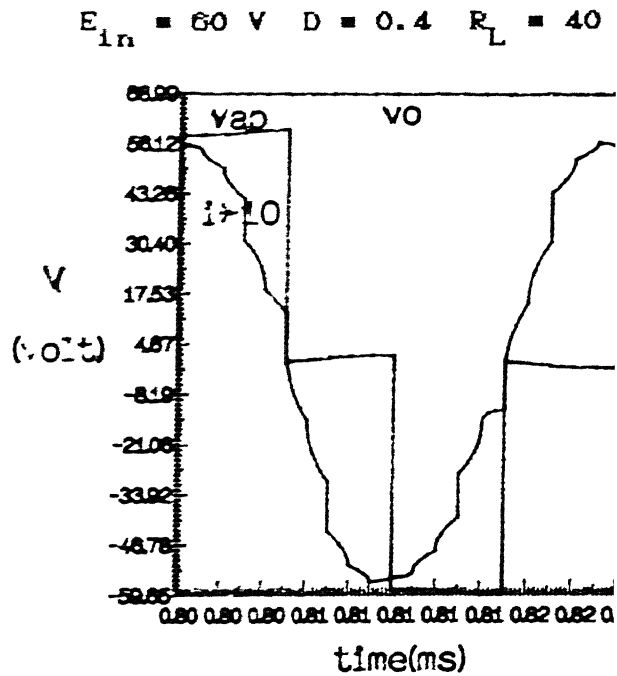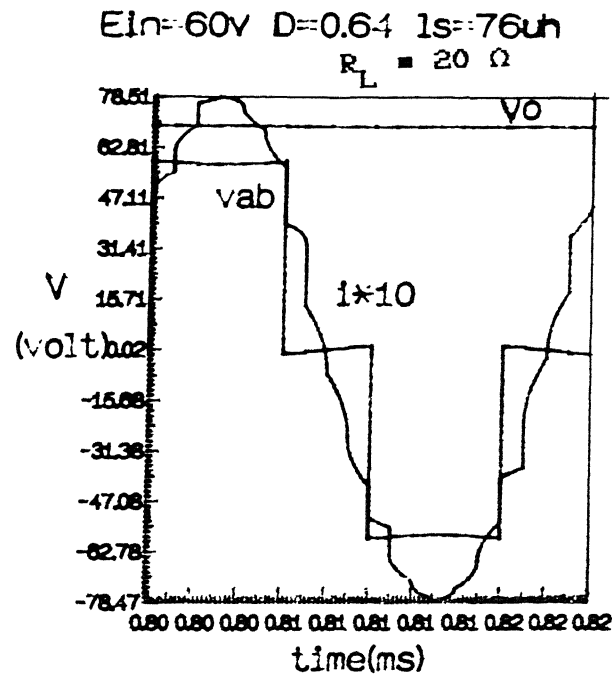
Fig. 4.5 : Simulation waveform for D = 0.64 and D = 0.4 E_{in} = 60V

D=0.41 RL=60ΩEin=60volt

V
Volt

time(ms)

D=0.4 Ein=60v RL=80ohm

V
Volt

time(ms)

V
Volt

time(ms)

V
Volt

time(ms)
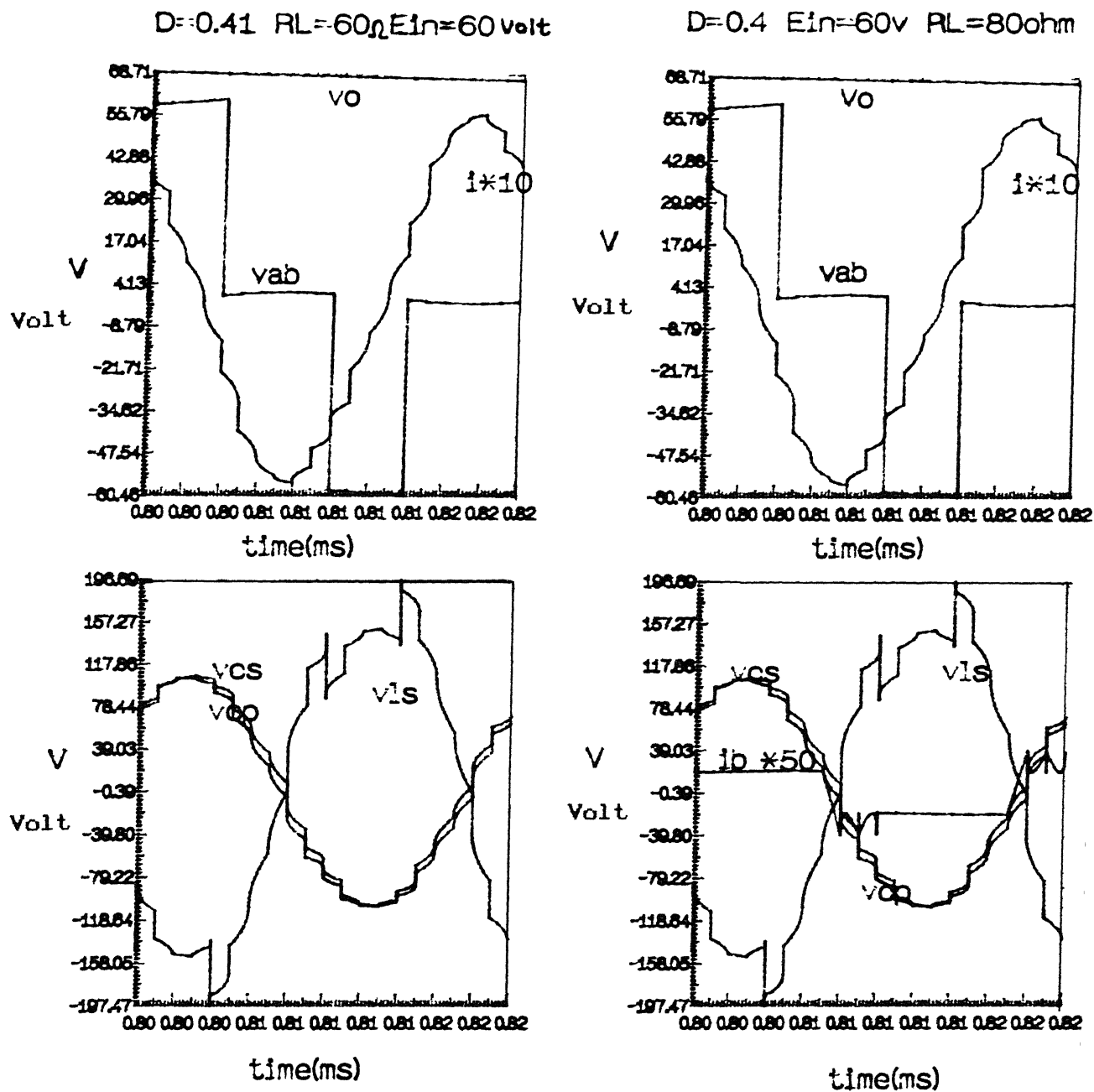
Fig. 4.6 : Simulation waveforms for D=0.41 and D=0.4 E_{in} = 60V

CHAPTER 5

DESIGN AND IMPLEMENTATION

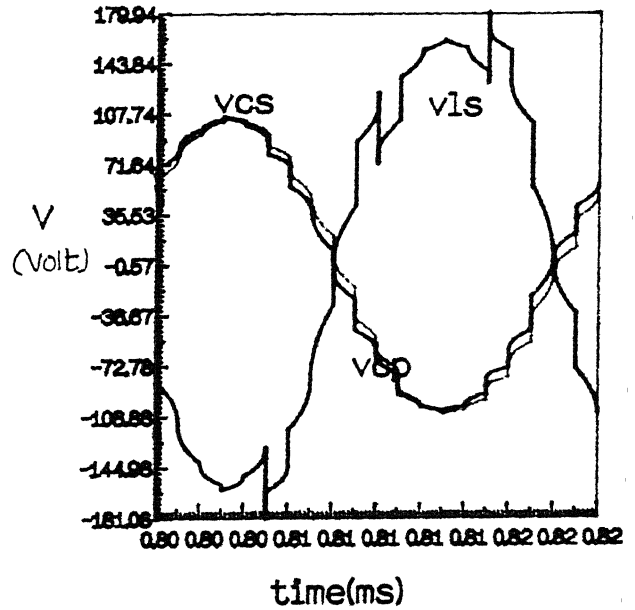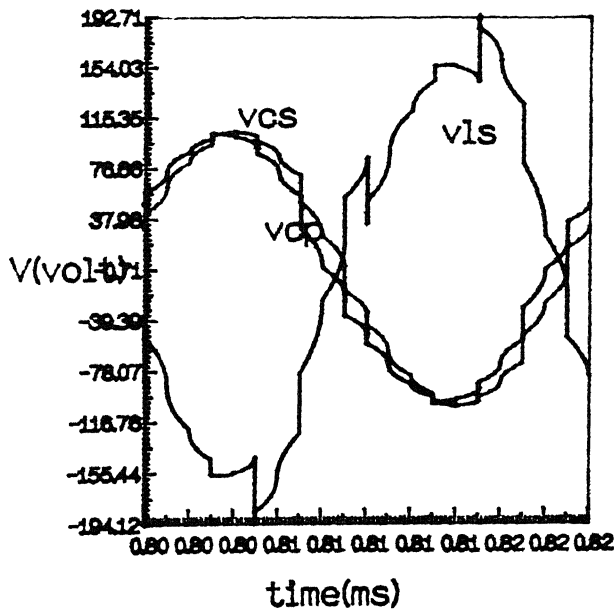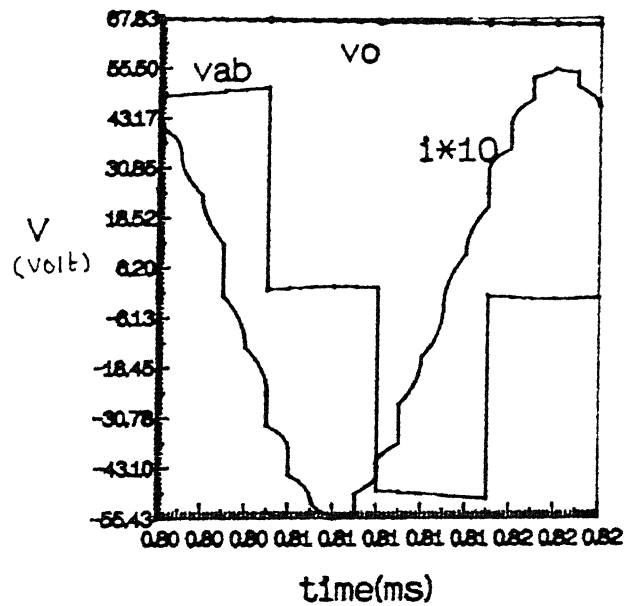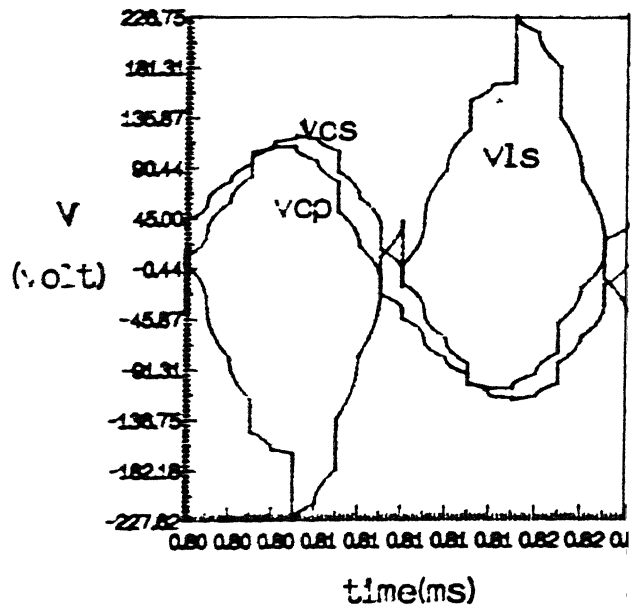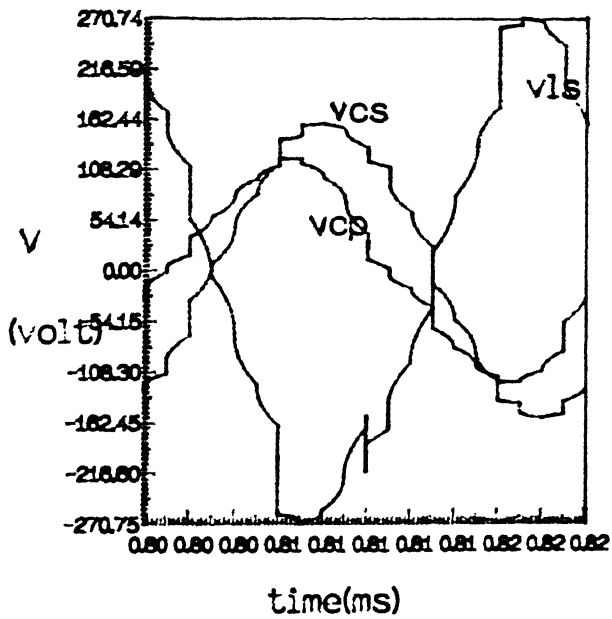In this chapter some guide lines are given for the selection of component values and their ratings are given with an illustrative example.

5.1 DESIGN

Design curves are shown in Figs. 3.3 to 3.7 which are obtained by the analysis presented in chapter 3. LCC resonant converter attempts to take advantage of the best characteristics of the series and the parallel converter while eliminating their weak points (lack of no load regulation for the series-resonant converter and circulating current independent of load for the parallel-resonant converter). This goal is met by proper selection of the resonant component.

By viewing the characteristics gain curve Fig. 3.9, it is clear that the converter can operate and regulate at no load provided that the parallel-resonant capacitor C_p is not too small. If m (C_s/C_p) increases from 1 to 2, the characteristics of the LCC resonant converter approach that of the SRC. Thus smaller the C_p is, the less "selectivity" is available in the resonant curves.

It is also observed that as the ratio 'm' increases the variation in duty ratio required to keep the output voltage constant also increases [3]. Thus for the regulation of the output voltage, the duty ratio has to be varied over larger range for m=2, compared to m=1. From these considerations, it is felt that m=1 is satisfactory.

Appropriate selection of J (Normalized load current) results in minimum KVA rating of tank circuit per kW of output power and minimum peak inverter output current at full load. A proper choice of F (ratio of switching frequency to series resonance frequency) also results in reduced peak currents at light loads while maintianing lagging pf mode of operation.

From Fig. 3.3 to 3.7, the following values were found to be near optimum for the design example

$$\frac{C_s}{C_p} = 1, \quad J = 0.9, \quad M = 0.96, \quad F = 1.1$$

5.2   DESIGN EXAMPLE

After selection the design parameters as explained above, the converter is designed with the following specifications :

Power output   :   100 Watts

Minimum input voltage   :   50 Volts

Switching frequency   :   50 KHz

The converter gain, E_o/E_{in} :   0.9

Full load resistance $R_L = E_o^2/P$

$$= \frac{(0.9 \times 50)^2}{100}$$

$$= 20.25 \text{ ohms}$$

The values of L_s and C_s are calculated using (5.1) and (5.2)

$$L_s = \left[\frac{M\ J\ V_B^2}{P_o} \right] \left[\frac{F}{(2\pi f_s)} \right] \qquad (5.1)$$

$$C_s = \left[F\ P_o \right] / \left[(2\pi f_s)(MJV_B^2) \right] \qquad (5.2)$$

The values calculated for the design example are :

$$L_s = 76 \ \mu H$$

$$C_s = 0.16 \ \mu F$$

Since

$$m = \frac{C_s}{C_p} = 1, \qquad C_p = 0.16 \ \mu F$$

5.3 CONTROL CIRCUIT

Fig. 5.1 gives the detailed control circuit used to generate the trigger pulse at a frequency of 50 KHz. Pulsewidth control IC SG3524 is used to generate the main trigger pulse to MOSFETs S_1 and S_3. The delayed triggers for MOSFETs S_2 and S_4 are derived by comparing the saw tooth waveform (100 KHz) at Pin 7 of SG3524 with variable dc reference. Table I shows the list of the components used in the circuit. The rest of the circuit is self explanatory. Fig. 5.2 shows waveform from SG3524 and gating pulses for S_1-S_4.
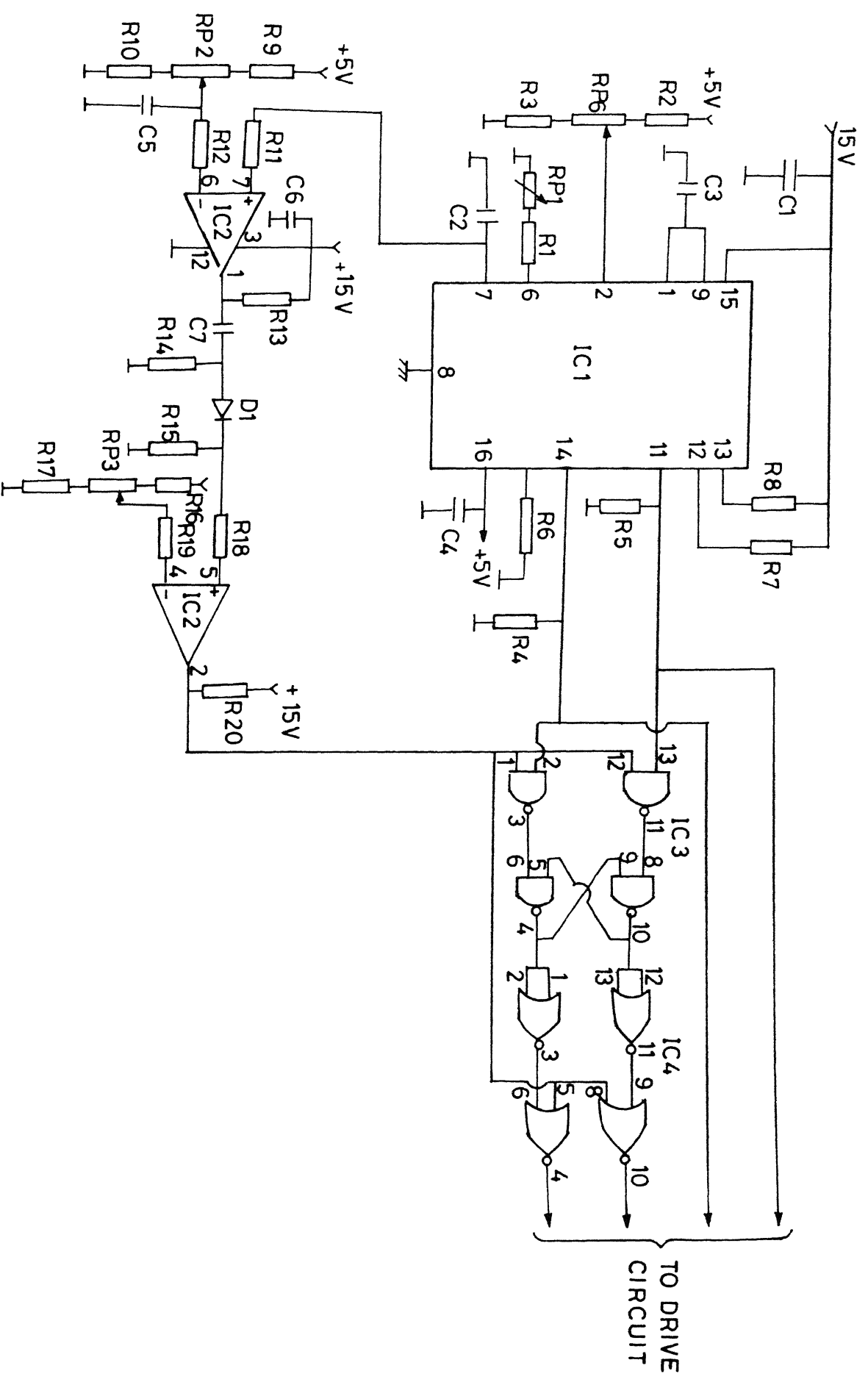
Fig.5·2 Detailed control circuit diagram

52

5.4 DRIVE CIRCUIT

Each MOSFET is driven by its own driver card which is floating at its source potential. Fig. 5.3 shows the detailed circuit diagram of the drive circuit. Optoisolator 6N134 is used to get the required isolation. The isolated power supplied of +5V and +12V are derived using regulator IC7805 and 7812 respectively. The ac voltage is stepped using small transformer and the voltage is rectified.

Fig.53 Detailed driver circuit circuit diagram

TABLE I

Part Number	Description	Part Number	Description
IC1	SG3524	C7	2.7PF
IC2	LM339	R2,R7,R8	1K
IC3	CD4011	R3	2.2K
IC4	CD4001	R4,R5,R6	56K
D1	1N4148	R9,R10	220Ω
RP1	1K	R18,R19,R11,R12	62K
RP2,RP3,RP4	2K	R1,R13,R20	1.5K
C1,C3,C4	0.1μF	R14	4.7K
C2	0.005μF	R15	10K
I5	0.22KPF	R16	6.2K
C6	100KPF	R17	820Ω

TABLE II

Part Number	Description	Part Number	Description
Q1	2N2222	R6	820Ω
Q2	SL100	R7	2.2K
Q3	SK100	R8	6.2K
D1,D2	1N4007	R9	1K
C2,C4	0.47μF/250V	R10	10K
C5	0.01μF	R11	26
C7,C8	0.1μF	R12	47K
C6	560PF	R5	1.5K
R2,R4	22K	C1,C3	470μF/50V

CHAPTER 6

CONCLSUSIONS

6.1 CONCLUSIONS

A fixed frequency LCC (series-parallel) resonant converter has been analysed using the Fourier series aproach. This frequency domain analysis presented in this thesis considerably simplifies the steady state analysis by eliminating the need of solving differential equations. Analysis has been used to obtain design curves and a design example has been presented to illustrate the design procedure. Results obtained from SPICE simulation waveforms have shown the ability of the converter to regulate the output load voltage at different loads by varying the duty ratio (δ).

6.2 SUGGESTION FOR FURTHER WORK

For all loads converter is not showing lagging power factor mode of operation. By careful selection of various parameters and components a converter operating in above resonance mode (lagging pf) for all loads is possible.

APPENDIX A

PROGRAMME FOR SOLVING 'θ' BY NEWTON RAPHSON METHOD

```c
# include <stdio.h>
# include <stdlib.h>
# include <math.h>
# define sqr(a) a*a
main()
(
 float f,m,a;
 int n;
 int i,j,k;
 float cosp,sine,summ,term;
 float term1,term2,funct,deriv;
 system("clear");
 printf ("\n ENTER THE VALUES OF F,a AND M \n");
 printf ("\n F :");
 scanf ("%f",&f);
 printf ("\n a :");
 scanf ("%f",&m);
 printf ("\n M :");
 scanf ("%f",&a);
 printf ("\n UPPER LIMIT IS :");
 scanf ("%d",&n);
 cosp = a*(1+(f*f -1)/m);
 printf ("\n cos(theta)    ==  %f",cosp);
 summ = cosp;
 term1 = cosp/(sqr(f)-1);
 term2 = a*(sqr(f)+m-1)/(m*(sqr(f) -1));
 i = 3;
 deriv = 0.0
 while (1 < n-1)
 (
   sine = sqrt(1-cosp*cosp);
   funct = term1 - term2;
   deriv = deriv + ((1-2)*sine)/(1-((1-2)*(1-2)*sqr(f)));
   cosp = summ - (funct/deriv);
   term1 = term1 + cosp/((sqr(i)*sqr(f)) -1 );
   term2 = term2 + a*((sqr(i)*sqr(f))+m-1)/(m*((sqr(i)*sqr(f))
   summ = cosp;
   printf ("\n cos(%d*theta)  == %f",i,cosp);
   i = i + 2;
 )
)
```

PROGRAMME FOR SOLVING I $_{Lspn}$

```c
#include <stdio.h>
#include <math.h>

main()
(
int p,1;
double f,θ,j,m;

printf("Enter p:");
scanf("%d",&p);
printf("\nEnter f:");
scanf("%f",&f);
printf("\nEnter theta:");
scanf("%f",&%);
printf("\nEnter m:);
scanf("%f",&m);

j=0.0;

for(i=1;1(=p;1++)
j=j+((1+m*m-(2*m*cos((2*p-1)*θ)))/((2*p-1)*(2*p-1)*f*f-1));
j=j*0.9;
printf("\nvalue of final j %f", j);
)
```

PROGRAMME FOR SOLVING NORMALIZED LOAD CURRENT (J)

```c
#include (stdio.h)
#include (math.h)

main()
(
int p,i;
double f,θ,j;

printf("Enter p :");
scanf("%d",&p);
printf("\nEnter f:");
scanf("%f",&f);
printf("\nEnter theta:");
scanf("%f",&θ);
j=0.0;

for(i=1;1(=p;1++)
j=j+((sin((2*p-1)*θ))/((2*p-1)*((2*p-1)*(2*p-1)*f*f-1)));
j=j*8*f/(3.14*3.14);
printf("\n value of final j %f",j);
```

LCC RESONANT CONVERTER SIMULATION CIRCUIT

```
vdc 19 13 50
v1 19 12 0
*MOSFET INVERTER BRIDGE
vs1 12 14 0
m1 14 15 1 1 switch
m2 0 18 13 13 switch
m3 1 16 13 13 switch
m4 12 17 0 0 switch
d1 1 14 drec
d3 0 12 drec
d4 13 0 drec
rc1 15 0 100meg
rc2 16 0 100meg
rc3 17 0 100meg
rc4 18 0 100meg
vg1 15 1 pulse(0 10 0 2n 2n 9.996u 20u)
vg2 18 13 pulse(0 10 18u 2n 2n 9.996u 20u)
vg3 16 13 pulse(0 10 10u 2n 2n 9.996u 20u)
vg4 17 0 pulse(0 10 8u 2n 2n 9.996u 20u)
*RESONANT NETWORK
cs 1 2 0.16u  1c=0
rs 2 3 1m
vs 3 4 0
1 4 5 76u        1c=0
cp 5 0 0.16u                  1c=0
vb 5 6 0
*DIODE BRIDGE RECTIFIER
d11 6 7 drec
d21 8 6 drec
d12 0 7 drec
d22 8 0 drec
ro 7 9 1m
lo 9 10 5m
vo 10 11 0
co 11 8 5u 1c=0
r1 11 8  18
*additional element
re1 2 0 100meg
re2 1 0 100meg
re3 5 0 100meg
re5 3 0 100meg
re6 9 0 100meg
re7 10 0 100meg
re8 19 0 100meg
re9 13 0 100meg
re10 15 0 100meg
```

```
.model switch nmos(level=1 vto=3 kp=1
.model drec d(tt=100n)
.tran 0.1u 320u 300u u1c
.print v(1) v(1)-v(2)
.end
```

REFERENCES

[1]   Vorperian V. and Slosodan Cuk, "A complete dc analysis of the series resonant converter," IEEE Power Electronics Specialists Conference, 1982 Record, June 1982, pp 85-100.

[2]   Stevem D. Johnson and Robert W. Erickson, "Steady state analysis and design of the parallel resonant converter," IEEE Trans. on Power Electronics, Vol.3, No.1, June 1988, pp 93-102.

[3]   R.L. Steigerwald, "A comparison of half bridge resonant converter topologies," IEEE Trans. on Power Electronics, Vol. 3, No. 2, April 1988, pp 174-182.

[4]   S.D.Johnson, A.F.Witulski and E.W.Erickson, "A comparison of resonant topologies in high voltage DC applications", IEEE Trans. on Aerospace and Electronics System, Vol. 24, No. 3, May 1988, pp 263-273.

[5]   D.M. Divan and Gray Skibinski, "Zero switching loss inverter for high power applications", IEEE Trans.Industry Application, Vol. IA-25, No. 4, July/Aug 1989, pp 633-643.

[6]   J.B. Klassens, "DC-AC series resonant converter system with high internal frequency generating multiphase ac waveforms for multi kilowatt power levels," IEEE Trans. Power Electronics Specialists Conference, 1985 Record, pp 204-213.

[7]   Boris S. Jacobson and Thomos A-Well, "Sequential switching series resonant converter with phase shift control", IEEE Applied Power Electronics Conference, 1988, pp 190-199.

[8]   F.G. Turnbull and R.E. Tompkins, "Design of a pulse width modulated resonant converter for high output voltage power supply," IEEE Industry Applications Society Annu. Meeting, 1985 Record, pp 1145-1150.

[9]   F.C. Schwarz, "An improved method of resonant current pulse modulation for power converters," IEEE Applied Power Electronics Conference, 1987 Proc., pp 35-144.

[10]   J.G. Hayes, N. Mohan and C.P. Henze, "Zero-voltage switching in a constant frequency digitally controlled dc-dc converter," IEEE Applied Power Electronics Conference, 1988 Record, pp 360-366.

[11]   GYU B. Joung, Chun T. Rim and GYU H. Cho, "Integral cycle mode control of the series resonant converter," IEEE Trans. on Power Electronics, Vol. 4, No.1, Jan. 1989, pp 83-91.

[12]   GYU B. Joung, Jung G. Cho and GYU H. Cho, "Generalised quantum resonant converters using a new concepts of quantum reso- nant switch," IEEE Applied Power Electronics Conference, 1990, pp 847-854.

[13]   Rudolf P. Severns, "Topologies for three element resonant converter," IEEE Trans. on Power Electronics, Vol. 7, No. 1, pp 89-98, Jan. 1992.

[14]   AKS Bhat, "A unified approach for the steady state analysis of resonant converters," Proceedings of International Conference on Power Electronics, Tokyo, April 1990, pp 191-197.

[15] AKS Bhat, "Analysis and design of a fixed frequency LCL type series resonant converter," IEEE Applied Power Electronics Conference Record, 1992, pp 253-260.

[16] AKS Bhat, "Analysis and design of a modified series resonant converter," IEEE Applied Power Electronics Conference Record, 1991, pp 594-600.

[17] S. Deb, A. Joshi and S.R. Doradla, "A novel frequency-domain model for a parallel resonant converter," IEEE Trans. on Power Electronics, Vol.3, No. 2, April 1988, pp 1163-1172.

[18] P.P. Roy, S.R. Doradla and S. Deb, "Analysis of the series resonant converter using a frequency domain model," IEEE PESC, 1991, pp 482-489.

[19] AKS Bhat, "Frequency domain analysis of a fixed frequency LCL type series resonant converter," International Power Electronics and Motion Control Conference, June 1994.

[20] AKS Bhat, "Analysis and design of LCL type series resonant converter," IEEE INTELEC, 1990, pp 172-178.

[21] Sujoy Deb, A. Joshi and S.R. Doradla, "A novel frequency domain model for a parallel resonant converter," IEEE Trans. on Power Electronics, Vol. 3, No. 2, April 1988.